BMC Biophysics

RESEARCH ARTICLE Open Access

Characterizing low affinity epibatidine binding to α4β2 nicotinic acetylcholine receptors with ligand depletion and nonspecific binding

Alexandra M Person[1] and Gregg B Wells[1,2,3*]

Abstract

Background: Along with high affinity binding of epibatidine (K_{d1}≈10 pM) to α4β2 nicotinic acetylcholine receptor (nAChR), low affinity binding of epibatidine (K_{d2}≈1-10 nM) to an independent binding site has been reported. Studying this low affinity binding is important because it might contribute understanding about the structure and synthesis of α4β2 nAChR. The binding behavior of epibatidine and α4β2 AChR raises a question about interpreting binding data from two independent sites with ligand depletion and nonspecific binding, both of which can affect equilibrium binding of [^{3}H]epibatidine and α4β2 nAChR. If modeled incorrectly, ligand depletion and nonspecific binding lead to inaccurate estimates of binding constants. Fitting total equilibrium binding as a function of total ligand accurately characterizes a single site with ligand depletion and nonspecific binding. The goal of this study was to determine whether this approach is sufficient with two independent high and low affinity sites.

Results: Computer simulations of binding revealed complexities beyond fitting total binding for characterizing the second, low affinity site of α4β2 nAChR. First, distinguishing low-affinity specific binding from nonspecific binding was a potential problem with saturation data. Varying the maximum concentration of [^{3}H]epibatidine, simultaneously fitting independently measured nonspecific binding, and varying α4β2 nAChR concentration were effective remedies. Second, ligand depletion helped identify the low affinity site when nonspecific binding was significant in saturation or competition data, contrary to a common belief that ligand depletion always is detrimental. Third, measuring nonspecific binding without α4β2 nAChR distinguished better between nonspecific binding and low-affinity specific binding under some circumstances of competitive binding than did presuming nonspecific binding to be residual [^{3}H]epibatidine binding after adding a large concentration of cold competitor. Fourth, nonspecific binding of a heterologous competitor changed estimates of high and low inhibition constants but did not change the ratio of those estimates.

Conclusions: Investigating the low affinity site of α4β2 nAChR with equilibrium binding when ligand depletion and nonspecific binding are present likely needs special attention to experimental design and data interpretation beyond fitting total binding data. Manipulation of maximum ligand and receptor concentrations and intentionally increasing ligand depletion are potentially helpful approaches.

Background

Ligand depletion can significantly affect estimates for dissociation (K_d) or inhibition (K_i) constants from equilibrium binding data of epibatidine (EB) and α4β2 nicotinic acetylcholine receptor (nAChR) because of the high affinity of EB (K_{d1}≈10 pM). Errors from ligand depletion arise from inappropriately assuming that free ligand concentration equals total ligand concentration while using total ligand concentration as the independent variable for modeling the binding data. The assumption is attractive because total ligand concentration as the independent variable is suitable for least squares fitting of binding data [1,2]. Ligand depletion can be minimized when designing binding experiments with EB and α4β2 nAChR. Radiolabeled EB with higher specific activity (for example, ^{125}I instead of ^{3}H) can lead to less ligand depletion by allowing

* Correspondence: gbwells@tamu.edu
[1]Department of Molecular and Cellular Medicine, Texas A&M University System Health Science Center, College Station, TX 77843-1114, USA
Full list of author information is available at the end of the article

a smaller concentration of α4β2 nAChR to produce useful data. A larger reaction volume at a fixed mole quantity of α4β2 nAChR reduces ligand depletion by reducing the difference between free and total concentration of radiolabeled EB. These avoidance strategies based on design of experiments, however, might be difficult to use in some situations. For example, a newly developed and ^{3}H-labeled EB derivative might be available only with low specific activity. Large reaction volumes might be impractical for numerous samples associated with high throughput screening [3]. When ligand depletion cannot easily be avoided, how can data with both ligand depletion and nonspecific binding (NSB) be correctly interpreted from EB and α4β2 nAChR?

Effects of ligand depletion on binding data have long been recognized, leading to models that correctly include ligand depletion with single and multiple specific binding sites [3-9]. For [^{3}H]EB, a ligand with relatively low specific activity, and α4β2 nAChR, ligand depletion has been recognized and avoided as a potentially confounding factor for interpreting binding data [10-17]. Alternatively, one site and two sites models for estimating binding constants have included ligand depletion with negligible NSB [18]. Combining ligand depletion and NSB, however, imposes additional demands on binding models. For example, specific binding cannot be calculated simply by subtracting NSB from total binding. Instead, a binding model including both ligand depletion and NSB must fit total binding [6] as has been shown with one specific binding site [19]. In addition to the high potency or high affinity site, functional data from electrophysiology and $^{86}Rb^{+}$ flux [20-41] and binding data [12,18,20,42,43] for α4β2 or α4β2-containing nAChR suggest a second, low potency or low affinity specific binding site. The difference in agonist potency at the two sites in functional assays has been attributed to α4β2 nAChR with different α:β stoichiometries [21,25,28,30,33]. $(\alpha4)_2(\beta2)_3$ contributes high potency and $(\alpha4)_3(\beta2)_2$ contributes low potency. Binding data from our laboratory suggest two independent sites and not two cooperative sites [18]. The physical basis of low affinity equilibrium binding of [^{3}H]EB detected under some conditions and the relationship between the low affinity site observed by equilibrium binding and the low potency site observed by functional methods are not known. On the other hand, a single binding site has been suggested for α4β2 nAChR [12,14] and for extracellular domain α4β2 nAChR [18] from binding data. Photolabeling of α4β2 with [^{3}H]EB also identified a single binding site [44]. Models of α4β2 nAChR binding data, therefore, should not assume the presence of high and low affinity sites. Instead, an interpretation of binding data needs to test the hypothesis of one binding site versus more than one binding site.

How does interpreting binding data with ligand depletion with NSB and a single binding site [19,45] need to be modified when a second, low-affinity specific binding site might be present from α4β2 nAChR? Detecting and accurately interpreting properties of the low affinity site is important because of the potential biological relevance of the low-affinity specific site. The low affinity binding site might reflect biologically important roles for α4β2 nAChR, reflect a variant structure of the agonist binding site, or give insight into the assembly of α4β2 nAChR. The goal of this study was to determine, using computational modeling, whether fitting total binding is sufficient for characterizing the low affinity binding site from α4β2 nAChR in the context of ligand depletion and NSB. The modeling simulated saturation binding, homologous competition, and heterologous competition. The experimental foundation for the modeling was reported previously with K_{d1} = 13 pM for the high affinity site and K_{d2} = 12 nM for the low affinity site [18]. The findings are potentially relevant to other ligands and receptors when two or more specific binding sites are possible and when ligand depletion and NSB affect binding data.

Methods

Equations of the models

For an introduction to interpreting equilibrium binding with ligand depletion and NSB, see Swillens [19] and Motulsky and Christopoulos [7]. The models of saturation binding and homologous and heterologous competition were based on mass action equations and conservation of mass (Figure 1). Figure 1 shows the notations for the states and equations for the equilibrium dissociation and inhibition constants of the models. Equations for a model were solved numerically within a Microsoft Excel environment using the Maple version 13 or 14 (Maplesoft) add-in. Parameters of a model were optimized to simulated data with the method of least squares using Excel and the Premium Solver Platform (Frontline Systems). Values of parameters were constrained to physically valid values.

Analytical solutions of cubic equations are available that describe ligand depletion (with and without NSB) of two binding sites and one ligand or of two sites with homologous competition [3,9,18,46,47]. Analytical solutions of a quartic polynomial describing ligand depletion and NSB of three binding sites and one ligand or of two binding sites with homologous competition can be derived from the general solution of a quartic polynomial [48]. Numerical solutions were used in this investigation because of the relative ease of implementation and the usefulness of numerical solutions when roots of quintic and higher order polynomials are needed to describe ligand depletion but for which analytical solutions are not available. For example, roots of a sixth order polynomial are needed to

Saturation binding for 2 sites

$$R1 + L \rightleftharpoons R1L \quad (a)$$

$$R2 + L \rightleftharpoons R2L \quad (b)$$

$$K_{d1} = \frac{R1 * L}{R1L} \quad (c)$$

$$K_{d2} = \frac{R2 * L}{R2L} \quad (d)$$

$$R1T = R1 + R1L \quad (e)$$

$$R2T = R2 + R2L \quad (f)$$

$$LT = R1L + R2L + L + \alpha_L * L \quad (g)$$

$$NSB_L = \alpha_L * L \quad (h)$$

unknowns: R1, R2, L, R1L, R2L

parameters: K_{d1}, K_{d2}, R1T, R2T, α_L

Homologous or heterologous displacement for 2 sites

$$R1 + L \rightleftharpoons R1L \quad (i)$$

$$R2 + L \rightleftharpoons R2L \quad (j)$$

$$R1 + B \rightleftharpoons R1B \quad (k)$$

$$R2 + B \rightleftharpoons R2B \quad (l)$$

$$R1T = R1 + R1L + R1B \quad (m)$$

$$R2T = R2 + R2L + R2B \quad (n)$$

$$LT = R1L + R2L + L + \alpha_L * L \quad (o)$$

$$BT = R1B + R2B + B + \alpha_B * B \quad (p)$$

$$NSB_L = \alpha_L * L \quad (q)$$

$$NSB_B = \alpha_B * B \quad (r)$$

unknowns: R1, R2, R1L, R1B, R2L, R2B, B, L

parameters: K_{d1}, K_{d2}, K_{i1}, K_{i2}, R1T, R2T, α_L, α_B

Figure 1 Equations for the binding models are based on the law of mass action and conservation of mass. Two mass action equations (c)-(d) for dissociation constants derived from (a)-(b) and three conservation of mass equations (e)-(g) formed the five equations solved simultaneously for the two sites model$_{total}$ for saturation binding. Four mass action equations for dissociation constants derived from (i)-(l) and four conservation of mass equations (m)-(p) formed the eight equations solved simultaneously for the two sites model$_{total}$ for homologous or heterologous competition. L was the independent variable for two sites model$_{free}$ for saturation binding, which did not include Eq. (g). B was the independent variable of two sites model$_{free}$ for competition, which did not include Eq. (p). One site model$_{total}$ excluded terms referring to the second site. The two sites model for saturation binding that ignored ligand depletion was based on Eqs. (c)-(f) and assumed LT = L. Notation: α_L = constant describing NSB of radioligand; K_{d1} = dissociation constant of high affinity binding site; L = free radioligand; LT = total radioligand; NSB_L = nonspecific binding of radioligand; R1 = unbound first binding site; R1L = radioligand bound to first site; R1T = total high affinity binding site; B = free competitor (blocker). With analogous notations, the index "2" in these equations refers to the low affinity binding site.

describe heterologous competition with two sites and ligand depletion and NSB, which precludes an analytical solution.

Data generation and model fitting

True binding behaviors (i.e., noiseless data) were defined as the output from two-sites models using defined values of parameters and free ligand concentration as the independent variable (two sites model$_{free}$). Noise was superimposed by adding, to each noise-free data point, a random number selected from a standard normal distribution with a constant standard deviation (SD) determined by context. The SD value was constant along the *x*-axis. In some cases, noise was described by the maximum signal to noise ratio (S/N). The SD for noise was the maximum signal in the noiseless data divided by the maximum signal to noise ratio (i.e., SD = (maximum signal)/(stated maximum S/N)). Multiple data sets with different SD values for noise were fitted simultaneously by weighting, by the inverse of the variance of the noise, the contribution of a data set to the sum of squares. Total concentration of added ligand was the independent variable for the one site model$_{total}$ and two sites model$_{total}$ when fitting noiseless and noisy data that included NSB. All results are displayed using total concentration on the *x*-axis. All ligand concentrations appearing in the text refer to total concentration unless otherwise noted. The two sites model for saturation binding that ignored ligand depletion assumed that LT = L. The two sites model of apparent specific saturation binding was based on equations (c)-(g) and assumed α = 0 in equation (g) (Figure 1). Apparent specific binding was the difference between total binding and apparent NSB. Apparent NSB was defined as NSB measured independently without $\alpha 4\beta 2$ nAChR and equaled $\alpha/(1+\alpha)$* (total [^{3}H]EB). The Hill equation (Eq. (1)) for characterizing binding data by fitting with SigmaPlot 11 was:

$$y = A_0 / \left(1 + (K_{0.5}/x)^n\right) \quad (1)$$

Data were generated with the following parameter values published by our laboratory [18] unless otherwise stated: K_{d1} = 0.013 nM and K_{d2} = 12 nM for [^{3}H]EB; K_{i1} = 0.84 and K_{i2} = 775 nM for nicotine; fraction of R1T = 0.84; fraction of R2T = 0.16 (see Figure 1 for notation). When a R1T concentration is stated, the corresponding R2T concentration is implied.

Statistics

The one site models for saturation binding and competition data were simpler cases of the two sites models, making these two types of models nested [7]. Qualities of fit of the two types of models, therefore, were compared with the F-test [49]. The level of significance for

hypothesis testing was 0.05. The confidence level for a confidence interval (CI) was 95%. CIs for dissociation constants and average p values were based on logarithmic values.

Results

Effects of ligand depletion and NSB on saturation binding to two specific sites

The two sites model$_{free}$ generated errorless binding data using free [^{3}H]EB as the independent variable to investigate how ligand depletion without NSB affected saturation binding behavior. Increasing the concentration of binding sites increased ligand depletion, shifted the total binding curve to the right, increased the steepness of the curve, and obscured the distinctive contour of the low affinity binding site (Figure 2A). The binding contour of the high affinity site began shifting noticeably to the right and showed an increasingly sharp bend at [^{3}H]EB = R1T as R1T increased beyond K_{d1} (0.013 nM) (Figure 2B). The binding contour of the low affinity site started shifting rightward as R1T approached K_{d2} (12 nM). The rightward shift in the binding curves with ligand depletion means that relying on $K_{0.5}$ as an estimate of K_d overestimates dissociation constants. Eq. (2)

$$K_{d1} = K_{0.5,high} - (R1T/2) \quad (2)$$

correctly estimated K_{d1} from the half-maximum for the high affinity site ($K_{0.5,\ high}$) when $K_{0.5,\ high}$ was distinct [5,50]. Eq. (2), however, became increasingly difficult to use as rightward shift of the binding curve from the high affinity site led to overlap with the binding curve from the low affinity site.

The two sites model$_{free}$ generated errorless binding data with both ligand depletion and NSB to investigate how combining NSB with ligand depletion affected binding behavior. The effect of NSB depended on the extent of ligand depletion. With negligible ligand depletion at R1T = 0.0001 nM (Figure 3A), NSB with $\alpha = 10^{-6}$ started obscuring the binding contour from the low affinity site. NSB with $\alpha = 10^{-3}$ obscured binding to the high affinity site. With significant ligand depletion at R1T = 0.3 nM (Figure 3B), NSB with $\alpha = 10^{-4}$ obscured the binding contour from the low affinity site. With extreme ligand depletion at R1T = 300 nM (Figure 3C), the contributions to total binding from the high affinity site and the low affinity site were not distinct even without NSB. NSB with $\alpha = 1$ obscured specific binding to the high affinity site. Increasing ligand depletion also affected how NSB depended on total [^{3}H]EB concentration. The leftward shift in NSB with each log unit increase in α was relatively uniform when ligand depletion was negligible at R1T = 10^{-4} nM (Figure 3D). The leftward shift in NSB with each log unit increase in α, however, became nonuniform when ligand depletion became large (Figure 3E; R1T = 0.3 nM) or extreme (Figure 3F; R1T = 300 nM).

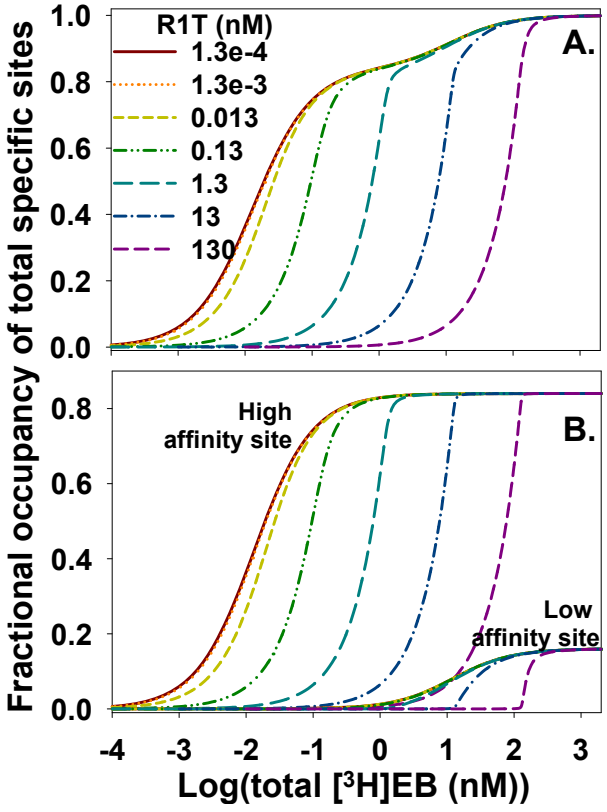

Figure 2 Ligand depletion shifts the binding curve rightward and obscures distinct features of the two binding sites. **A**. Fractional occupancy of total specific binding sites is shown at various concentrations of R1T. Increasing total binding sites increases ligand depletion, which shifts the total binding curve rightward. Ligand depletion also distorts the two sigmoidal features arising from binding to the high and low affinity sites. **B**. The fractional occupancies of high and low affinity sites are shown separately. The legend in A applies to B. Fractional occupancies of the low affinity site are clustered in the lower right corner of the plot. Only lines from R1T values of 13 and 130 nM are distinct for the low affinity site. The leftmost line from the low affinity site arises from overlap of the lines from the first five concentrations of binding sites. Binding was calculated with two sites model$_{free}$.

Modeling specific binding and NSB as total binding

How can dissociation constants be estimated when both ligand depletion and NSB contribute significantly to [^{3}H]EB binding? An effective approach when ligand depletion is negligible is to calculate specific binding as the difference between total binding and NSB measured without $\alpha4\beta2$ nAChR (apparent NSB). In accord with a one binding site model including ligand depletion and NSB [19], this approach was incorrect when ligand depletion was significant (Figure 3G and 3H). NSB shifted rightward from the apparent NSB as R1T increased because

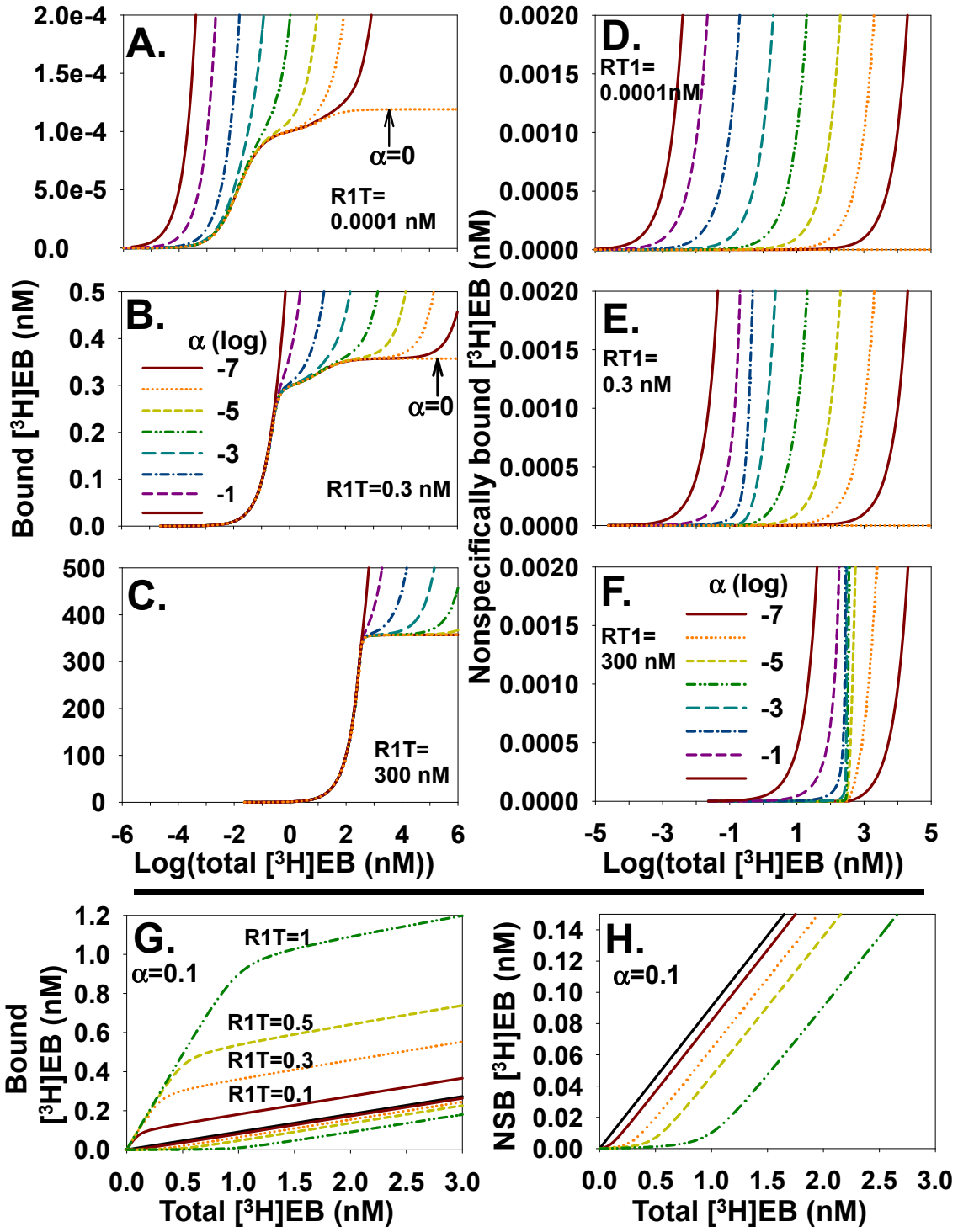

Figure 3 NSB depends on the extent of ligand depletion and cannot be calculated from apparent NSB. **A**. Total binding is shown when ligand depletion is negligible with increasing values of α ranging from 0 to 1 (integer log values of α from -7 to 0; legend for A-C in B). α = 0 is line with horizontal plateau at large concentration of [^{3}H]EB. **B** and **C**. Similar to A except ligand depletion is substantial (R1T = 0.3 nM) or extreme (R1T = 300 nM). The effects of a particular α value on total binding depend on the extent of ligand depletion. **D**, **E**, **F**. NSB on expanded *y*-scales shows how increasing ligand depletion affects NSB (legend for α in F; integer log values from -7 to 0). **G**. Specific binding is not calculated correctly as the difference between total binding and apparent NSB when ligand depletion is significant. Solid black line: apparent NSB obtained without α4β2 nAChR. Lines for total binding at increasing concentrations (nM) of R1T and, therefore, increasing ligand depletion appear above apparent NSB. Corresponding lines for NSB when α = 0.1 are below apparent NSB. **H**. NSB (same code for lines as in G) and apparent NSB (solid line) from G are shown with an expanded *y*-scale. Binding in this figure was calculated with two sites model$_{free}$.

increasing R1T decreased the free [^{3}H]EB concentration for a given total concentration of [^{3}H]EB. Subtracting apparent NSB from total binding led to calculated specific binding that was shifted rightward and downward compared to true specific binding (Figure 4A). This effect led to overestimating the values of K_{d1} and K_{d2} (Figure 4B and 4C), overestimating R1T (Figure 4D and 4E), and underestimating R2T (Figure 4D and 4E) as ligand depletion increased. The difference between total binding and NSB equals specific binding by definition. These results, however, showed NSB when α4β2 nAChR was present was not equal to NSB when α4β2 nAChR was absent (apparent NSB). Specific binding, therefore, did not equal the result of subtracting apparent NSB from total binding. This inequality arose because NSB with α4β2 nAChR present did not equal apparent NSB when ligand depletion was significant. This observation has been made previously for a one site model [19].

Specific binding and NSB of [^{3}H]EB and α4β2 nAChR needed to be modeled together as total binding using the two sites model$_{total}$. This conclusion was consistent with the findings from a general one site model [19]. Accuracy of the two sites model$_{total}$ for calculating saturation binding data was tested by comparing predicted [^{3}H]EB binding to [^{3}H]EB binding calculated with two sites model$_{free}$. The concentration of bound [^{3}H]EB calculated by the two methods agreed to at least fourteen significant digits across this range of parameters: 10^{-6} nM ≤ R1T ≤ 10^4 nM and 0 ≤ α ≤ 10^2 with 10^{-6} nM ≤ [^{3}H]EB$_{free}$ ≤ 10^6 nM. These results confirmed the accuracy of the binding calculations using the two sites model$_{total}$.

Potential for failing to identify low-affinity specific binding when modeling only total saturation binding

An important role for the two sites model$_{total}$ is to estimate dissociation constants and binding site concentrations from noisy binding data. These estimates, however, are valid only when the two sites model$_{total}$ fits data better than does the one site model$_{total}$ according to statistical testing. Under what circumstances are binding data from the two sites of α4β2 nAChR adequately explained by the one site model$_{total}$? In these situations, specific binding to the low affinity site is indistinguishable from high-affinity specific binding, NSB, or noise. On the other hand, what circumstances favor identifying the low-affinity specific binding site?

Deriving a computational expression for NSB from the general expression for binding to a single site suggested potential confusion between low-affinity specific binding and NSB as defined in Figure 1 (symbols similar to Figure 1):

$$K_d = \left(\frac{R}{RL}\right) * L_f \tag{3}$$

$$RL_{NSB} = \left(\frac{R_{NSB}}{K_{d,NSB}}\right) * L_f = \left(\frac{RT_{NSB}}{K_{d,NSB}}\right) * L_f \tag{4}$$

$$RL_{NSB} = NSB = \alpha * L_f \tag{5}$$

where $\alpha = (RT_{NSB}/K_{d,\ NSB})$ and $R_{NSB} = RT_{NSB}$ by the definition of homogeneous NSB. If NSB arises from a collection of heterogeneous sites, then

$$RL_{NSB,total} = \left(\frac{R_{NSB,1}}{K_{d,NSB,1}} + \frac{R_{NSB,2}}{K_{d,NSB,2}} + \cdots\right) * L_f \tag{6}$$

$$RL_{NSB,total} = \left(\frac{RT_{NSB,1}}{K_{d,NSB,1}} + \frac{RT_{NSB,2}}{K_{d,NSB,2}} + \cdots\right) * L_f \tag{7}$$

$$RL_{NSB,total} = NSB = \alpha * L_f \tag{8}$$

By analogy with these derivations, binding to the low affinity site also can be modeled as constant*L_f, similar to NSB, when R2≅R2T. On the other hand, low-affinity specific binding behaves differently from NSB when the approximation R2≅R2T fails. This approximation most likely fails as total [^{3}H]EB approaches its maximum concentration ([^{3}H]EB$_{max}$) in a saturation binding experiment. In contrast and by definition, R_{NSB}≅RT_{NSB} is valid for NSB; and NSB equals α*L_f at any [^{3}H]EB$_{max}$. When [^{3}H]EB$_{max}$ is sufficiently small that R2≅R2T is valid for the low-affinity specific binding site, the two sites model$_{total}$ does not fit significantly better than one sites model$_{total}$. This outcome supports the incorrect conclusion that a second low affinity site is not present. These observations led to the hypothesis that modeling total saturation binding data with ligand depletion and NSB can blur the important biological distinction between low-affinity specific binding and NSB for [^{3}H]EB and α4β2 nAChR.

Three approaches to characterizing the low-affinity specific binding site with saturation binding

To test this hypothesis, the one site model$_{total}$ was compared to the two sites model$_{total}$ by fitting noisy total binding data from the two sites model$_{free}$ with zero NSB (α = 0). The data (60 data points and 20 total concentrations of [^{3}H]EB) with R1T = 0.13 nM and [^{3}H]EB$_{max}$ = 2 nM were generated with the two sites model$_{free}$ and an unrealistically large maximum signal-to-noise ratio (S/N) of 13,300 (SD = 1 × 10^{-5} nM). The two sites model$_{total}$ fitted the data significantly better than the one site model$_{total}$ (p values of 1.5 × 10^{-24}, 2.2 × 10^{-22}, and 1.3 × 10^{-20}

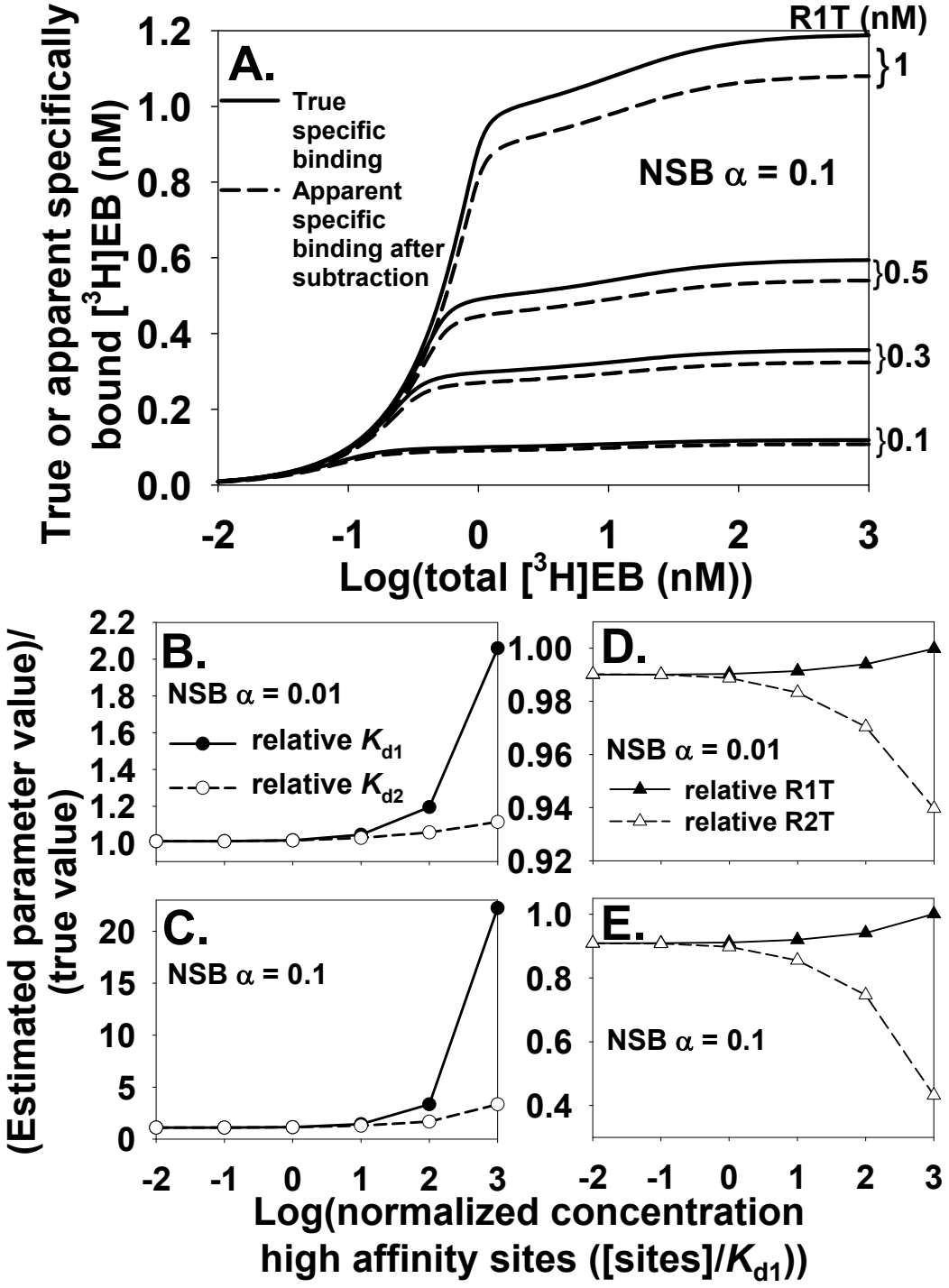

Figure 4 Calculating specific binding by subtracting apparent NSB from total binding of [^{3}H]EB to α4β2 nAChR leads to errors in estimating dissociation constants and binding site concentrations. **A**. Apparent specific binding (dashed lines) calculated by subtracting apparent NSB (α = 0.1) from total binding is less than the true specific binding (solid lines). These errors in specific binding lead to errors in estimating K_{d1} and K_{d2} (**B** and **C**) and R1T and R2T (**D** and **E**) from a two sites model that includes ligand depletion but excludes NSB. B and D were obtained with α = 0.01; C and E were obtained with α = 0.1. The *x*-axis in B-E is an index of ligand depletion. Binding data shown or used in this figure were calculated with two sites model$_{free}$.

for three trials). This result showed that fitting high precision total binding data with the two models identified low-affinity specific binding.

Reducing the precision of the data was expected to make detection of binding to the low affinity site more difficult. To test this expectation, binding data with the same R1T and $[^3H]EB_{max}$ were generated with a tenfold smaller but still unrealistically large maximum S/N of 1,330 (SD = 1×10^{-4} nM). Under these conditions, the two sites $model_{total}$ did not fit the data significantly better than the one site $model_{total}$ with five of five data sets (p = 0.33, 0.13, 0.24, 0.73, and 1.0). Fitting noisier data led to the misleading conclusion that only one specific binding site plus NSB satisfactorily accounted for the total binding data.

How can low-affinity specific binding be distinguished more reliably from NSB as S/N values decrease to realistic levels? Eqs. (3)-(5) suggested increasing $[^3H]EB_{max}$ so the approximation R2≅R2T no longer would be valid near $[^3H]EB_{max}$. The approximation would break down because increased binding of [^{3}H]EB to R2 at large values of [^{3}H]EB would cause a significant decrease in R2 as [^{3}H]EB approaches the increased value of $[^3H]EB_{max}$. To determine whether increasing $[^3H]EB_{max}$ helped distinguish the low affinity binding site from NSB in the presence of ligand depletion, the one site $model_{total}$ and the two sites $model_{total}$ were fitted to noisy data with zero NSB and with $[^3H]EB_{max}$ increased from 2 nM (60 data points) to 5 nM (63 data points). The maximum S/N of the data again was 1,330 (SD = 1×10^{-4} nM). With $[^3H]EB_{max}$ = 5 nM, the two sites $model_{total}$ fit better than the one site $model_{total}$ in five of five data sets ($p = 4.6 \times 10^{-11}$, 1.8×10^{-9}, 2.8×10^{-9}, 2.5×10^{-9}, and 1.7×10^{-12}). Increasing the data points from 60 to 63 did not account for this improved detection of low-affinity specific binding. Instead, this result was consistent with a breakdown of the approximation R2≅R2T as $[^3H]EB_{max}$ increased, leading to better discernment of binding at the low affinity site at $[^3H]EB_{max}$ = 5 nM compared to 2 nM.

To explore whether larger values of $[^3H]EB_{max}$ could distinguish low-affinity specific binding from NSB in data with more realistic precision, the one site $model_{total}$ and two sites $model_{total}$ were fitted to noisy data (maximum S/N = 36; SD = 0.0041 nM) and zero NSB (α = 0) (Figure 5A). When $[^3H]EB_{max}$ was 10 nM, the two sites $model_{total}$ usually did not fit the data better than the one site $model_{total}$. As $[^3H]EB_{max}$ increased, the likelihood of better fitting by the two sites $model_{total}$ and the likelihood of support for the presence of the low affinity site also increased. At $[^3H]EB_{max}$ = 100 nM with fitting $_{total}$ binding data only, the two sites $model_{total}$ fitted the data better than the one site $model_{total}$ for all trials. The increase in data points with increasing $[^3H]EB_{max}$ did not account for this improved detection of low-affinity specific binding.

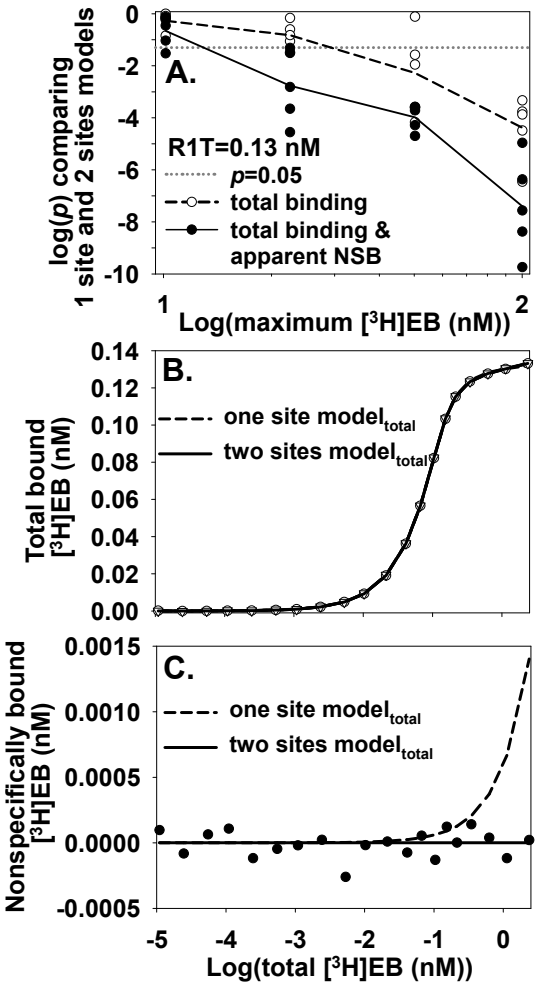

Figure 5 Increasing $[^3H]EB_{max}$ or simultaneously fitting apparent NSB helps identify low-affinity specific binding. **A**. Data sets with maximum S/N = 36 (SD = 0.0041 nM), R1T = 0.13 nM, α = 0, and various values of $[^3H]EB_{max}$ were fitted with one site $model_{total}$ and two sites $model_{total}$. The y-axis shows p values from comparisons. Total binding data only (○) or total binding along with apparent NSB (●) were fit. Dashed and solid lines connect averages of log(p) values. At $[^3H]EB_{max}$ = 100 nM and total binding only, the CIs included true values (K_{d1}, 11.9-14.0 pM, mean = 12.9 pM, K_{d2}, 3.4-12.2 nM, mean = 6.5 nM, R1T, 0.128-0.131 nM, mean = 0.129 nM; R2T, 0.014-0.021 nM, mean = 0.018 nM) (n = 5 for each CI). With $[^3H]EB_{max}$ = 22 nM and explicitly fitting apparent NSB, CIs included true values (K_{d1}, 10.6-13.2 pM, mean = 11.8 pM; K_{d2}, 3.9-17.4 nM, mean = 8.2 nM; R1T, 0.126-0.131 nM, mean = 0.128 nM; R2T, 0.020-0.023 nM, mean = 0.021 nM) (n = 5 for each CI). **B, C**. With zero NSB and highly precise data (SD = 1×10^{-4} nM), simultaneously fitting total binding data and apparent NSB helps identify low-affinity specific binding. Total binding data in B (40 points) were generated with R1T = 0.13 nM and $[^3H]EB_{max}$ = 2.37 nM. The one site $model_{total}$ and two sites $model_{total}$ appear to fit total binding data equally well up to $[^3H]EB_{max}$. The two sites $model_{total}$, however, fits apparent NSB values (●) in C significantly better than does the one site $model_{total}$, leading to $p = 2 \times 10^{-33}$ comparing models with simultaneous fitting. One site $model_{total}$: K_d = 0.014 nM, RT = 0.13 nM, $\alpha = 5.9 \times 10^{-4}$; two sites $model_{total}$: K_{d1} = 0.013 nM, K_{d2} = 10.5 nM, R1T = 0.013 nM, R2T = 0.022 nM, $\alpha = 1.0 \times 10^{-7}$.

As a second potential approach, fitting apparent NSB while simultaneously fitting total binding data might help distinguish low-affinity specific binding from NSB by directly evaluating NSB. To test this hypothesis, total binding data (40 data points) and apparent NSB binding data (20 data points) were generated with the same conditions (maximum S/N = 1,300; SD = 1×10^{-4} nM) that failed to distinguish the low affinity binding site with total binding data only. Simultaneously fitting total binding data (Figure 5B) and apparent NSB (Figure 5C) led to the two sites model$_{total}$ fitting the data significantly better than the one site model$_{total}$ in five of five data sets. The p values were vanishingly small ($p = 6.5 \times 10^{-31}$, 7.3×10^{-34}, 3.2×10^{-33}, 1.3×10^{-28}, and 2.1×10^{-33}). Figure 5C shows how fitting apparent NSB led to better detection of low-affinity specific binding. The one site model$_{total}$ could not fit total binding and simultaneously accurately fit the apparent NSB. In contrast, the two sites model$_{total}$ accurately fit the contribution from the low affinity site to total binding and simultaneously accurately fit the apparent NSB. With more realistic precision (maximum S/N = 36; SD = 0.0041 nM), the two sites model$_{total}$ usually fit the data better than did the one site model$_{total}$ for [^{3}H]EB$_{max}$ ≥ 22 nM (Figure 5A). In addition, simultaneously fitting both total binding and apparent NSB data more reliably identified low-affinity specific binding than did fitting only total binding. These results suggested that simultaneously fitting both total binding and apparent NSB could be superior to fitting only total binding for detecting low-affinity specific binding when NSB was negligible.

A third approach for potentially distinguishing low-affinity specific binding from NSB is based on how NSB varies with α4β2 nAChR concentration. Suppose, in an idealized case, that NSB arises solely from sources (e. g., walls of a test tube, surface of a glass filter, or a constant volume of cell membranes) that are independent of α4β2 nAChR. The independence of NSB from α4β2 nAChR suggests the hypothesis that varying α4β2 nAChR concentration helps distinguish low-affinity specific binding from NSB when ligand depletion is significant. Variation in α4β2 nAChR concentration could arise by injecting different amounts of cRNA into oocytes or by transfecting different amounts of cDNA into cells. To test this hypothesis, the one site model$_{total}$ and two sites model$_{total}$ with implicit fitting of NSB were fitted to noisy [^{3}H]EB binding data (maximum S/N = 36) generated at three different concentrations of α4β2 nAChR and with zero NSB (Figure 6A). The two sites model$_{total}$ consistently fit the data better than the one site model$_{total}$ for [^{3}H]EB$_{max}$ ≥ 22 nM (Figure 6B). In contrast, [^{3}H]EB$_{max}$ in the range of 100 nM was needed when the same numbers of data points were generated under similar conditions from a single α4β2 nAChR concentration (Figure 5A). These results suggested that simultaneous fitting of data from various α4β2 nAChR concentrations, when NSB is independent of α4β2 nAChR concentration, could help distinguish binding to the low affinity binding site better than fitting data from a single α4β2 nAChR concentration.

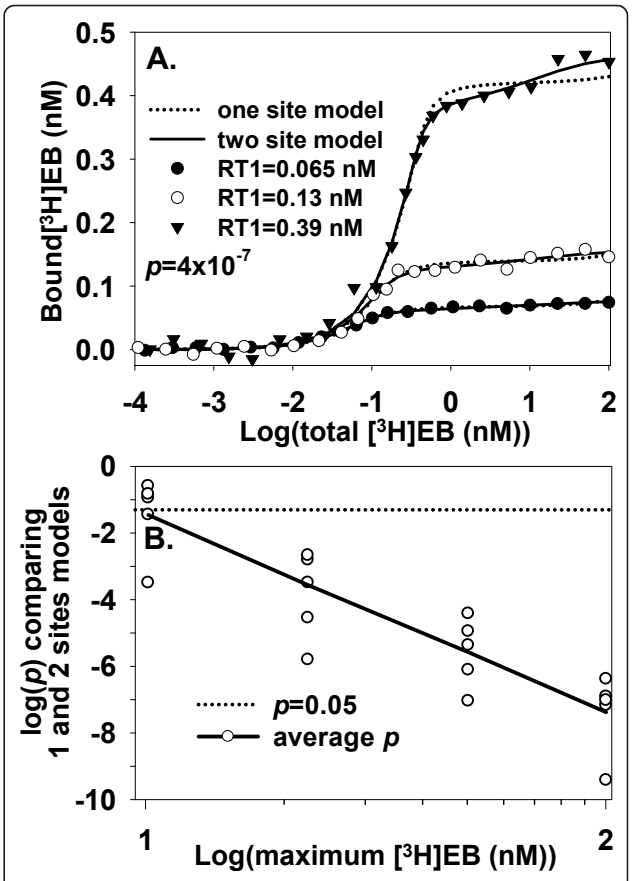

Figure 6 Simultaneously fitting binding data from several different concentrations of α4β2 nAChR identifies low-affinity specific binding. **A**. The one site model$_{total}$ and two sites model$_{total}$ with [^{3}H]EB$_{max}$ = 100 nM were fitted to noisy binding data with R1T = 0.065, 0.13, and 0.39 nM and α = 0. SD for noise at the R1T values was 0.002, 0.004, and 0.012, respectively (maximum S/N ratio≈36). The two sites model$_{total}$ shows a significantly better fit ($p = 4 \times 10^{-7}$). **B**. The y-axis shows p values for comparisons of one site model$_{total}$ and two sites model$_{total}$ from various [^{3}H]EB$_{max}$ values. The fitted data sets are analogous to the data sets shown in A; p-values from 5 data sets appear at each x-coordinate. Solid lines connect averages of log(p) values. The CIs of estimates of K_{d1} (9.2-18.5 pM; mean = 13.0 pM) and K_{d2} (1.0-1400 nM; mean = 38 nM) and R2T (0.015-0.66; mean = 0.34) (n = 5 for each CI) include true values.

Potentially, both sources independent of α4β2 nAChR concentration and sources correlated with α4β2 nAChR concentration might contribute significantly to NSB. The equation describing NSB in this case needs to include a component independent of ($RL_{NSB,\ indep}$) and a component dependent on α4β2 nAChR concentration

($RL_{NSB,\ dep}$). Based on Eqs. (3)-(5) and if $RT_{NSB,\ dep}$ is directly proportional to α4β2 nAChR, the relationship between NSB and free ligand becomes:

$$RL_{NSB,indep} + RL_{NSB,dep} = \left(\frac{R_{NSB,indep}}{K_{d,NSB,indep}} + \frac{R_{NSB,dep}}{K_{d,NSB,dep}}\right) * L_f \quad (9)$$

$$RL_{NSB,indep} + RL_{NSB,dep} \cong \left(\frac{RT_{NSB,indep}}{K_{d,NSB,indep}} + \frac{RT_{NSB,dep}}{K_{d,NSB,dep}}\right) * L_f \quad (10)$$

$$RL_{NSB,indep} + RL_{NSB,dep} \cong \left(\frac{RT_{NSB,indep}}{K_{d,NSB,indep}} + \frac{\beta * [\alpha 4\beta 2]}{K_{d,NSB,dep}}\right) * L_f \quad (11)$$

$$NSB_{total} = RL_{NSB,indep} + RL_{NSB,dep} \cong (\alpha_{ind} + \alpha_{dep} * [\alpha 4\beta 2]) * L_f \quad (12)$$

Eq. (12) for NSB_{total} or other expressions for $RT_{NSB,\ dep}$ can be incorporated into binding equations (Figure 1) when the low affinity binding site is investigated with various α4β2 nAChR concentrations and binding models.

Characterizing the low-affinity specific binding site by ligand depletion

How does combining NSB with ligand depletion affect the interpretation of saturation binding with ligand depletion? Without ligand depletion, large NSB tended to overwhelm the signal from the low affinity site when total and free [^{3}H]EB were high enough to populate the low affinity binding site (Figure 3A). Conditions leading to ligand depletion, however, would increase the concentration of the low affinity site, reduce free [^{3}H]EB and NSB, and lead to relatively more binding to the low affinity site than to NSB. With α = 0.1 and R1T = 0.00013 nM (negligible depletion), the ratio R2L/NSB was 1.1×10^{-5} at [^{3}H]EB = 12 nM and 4.4×10^{-6} at [^{3}H]EB = 50 nM. As expected, NSB overwhelmed the signal from the low affinity site at and above [^{3}H]EB = K_{d2}, which was the minimal concentration range needed to significantly populate the low affinity site. In contrast, with R1T = 20 nM (substantial depletion) and the low affinity site starting to participate in ligand depletion, the ratio R2L/NSB was much larger: 3.2 at [^{3}H]EB = 12 nM and 1.0 at [^{3}H]EB = 50 nM.

To test this promising usefulness for ligand depletion, noisy data (maximum S/N = 50 at each R1T) with α = 0.1 and significant ligand depletion at three values of R1T (0.13, 3, and 20 nM; $[^3H]EB_{max}$ = 0.15, 3.6, and 24 nM) were fitted by the one site $model_{total}$ and the two sites $model_{total}$. The two sites $model_{total}$ fit the data better in ten of ten trials and produced CIs that included the true values for the parameters (K_{d1} = 0.0133 nM, CI = 0.0120-0.0149 nM; K_{d2} = 11.9 nM, CI = 9.0-15.8 nM; fraction of low affinity site = 0.180, CI = 0.156-0.204; α = 0.098, CI = 0.092-0.103). To test the effect of simultaneously fitting apparent NSB, noisy data (maximum S/N = 50) with α = 0.1 at three values of R1T (0 nM for apparent NSB alone, 0.13, and 20 nM) were fitted by the one site $model_{total}$ and the two sites $model_{total}$. The two sites $model_{total}$ fit the data better in ten of ten trials and produced CIs including the true values for the parameters (K_{d1} = 0.0123 nM, CI = 0.0097-0.0156 nM; K_{d2} = 31.8 nM, CI = 6.5-155 nM; fraction of low affinity site = 0.291, CI = 0.133-0.450; α = 0.0997, CI = 0.0987-0.101). These results suggested that increasing ligand depletion might be useful for detecting and characterizing the low affinity site when NSB is significant in saturation binding data.

Effects of ligand depletion and NSB on homologous competition

To investigate effects of ligand depletion and NSB on homologous competition, a two sites $model_{free}$ and a two sites $model_{total}$ were developed using concentration of free or total cold EB as the independent variable (Figure 1B). Calculations of total binding using the two sites $model_{total}$ agreed with calculations with two sites $model_{free}$ to at least fourteen significant digits. The ranges of parameters tested were 1×10^{-6} nM ≤ R1T ≤ 1×10^{4} nM and 0 ≤ α ≤ 20 with 1×10^{-6} nM ≤ $[^3H]EB_{total} \le 1 \times 10^{6}$ nM. These results confirmed the accuracy of modeling homologous competition using total cold EB concentration as the independent variable.

Increasing ligand depletion by increasing R1T changed the appearance of homologous competition data using 0.013 nM [^{3}H]EB, which equaled the K_d for the high affinity binding site (Figure 7A). At R1T = 0.00013 nM, ligand depletion was negligible. The binding curve was symmetric about IC_{50} = 0.02612 nM with a Hill coefficient of -0.9995. The K_d calculated from a modified Cheng-Prusoff equation for homologous competition [51], which ignores ligand depletion:

$$IC_{50} = [^3H]EB + K_d \quad (13)$$

was 0.01316 nM, close to the value of K_d for the high affinity site. Increasing ligand depletion distorted the competition curve away from a sigmoidal shape and shifted the curve rightward. The curve at R1T = 130 nM was asymmetric about IC_{50} = 306 nM and did not follow Eq. (13). When [^{3}H]EB was increased to 13 nM, [^{3}H]EB concentration controlled IC_{50} when ligand depletion was negligible, agreeing with Eq. (13) (Figure 7B). IC_{50}, therefore, remained about 13 nM for R1T < 13 nM. Increasing ligand depletion shifted IC_{50} rightward when R1T ≥ 13 nM and made the homologous competition curves asymmetric around IC_{50}. These

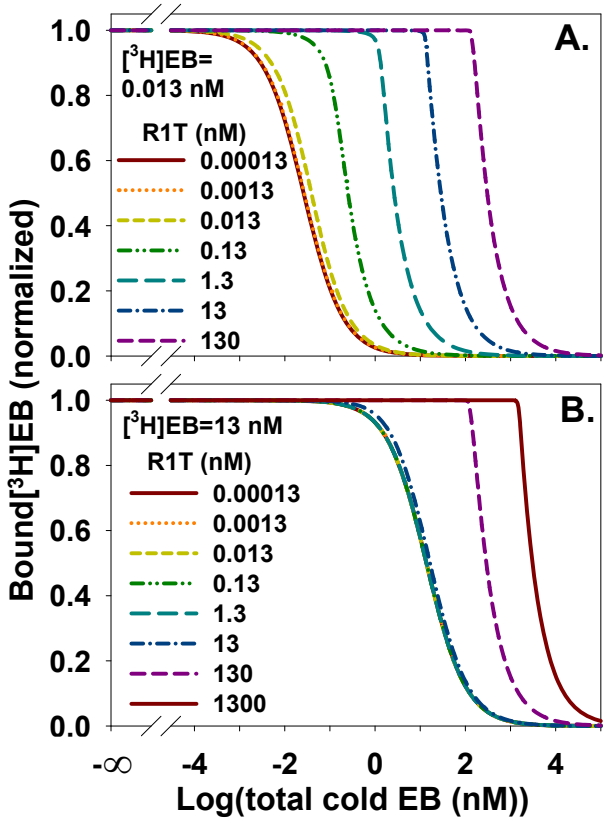

Figure 7 Ligand depletion affecting homologous competition data shifts IC_{50} rightward and distorts the sigmoidal shape of the competition curve. **A**. Homologous competition of 0.013 nM [^{3}H]EB and α4β2 nAChR at various concentrations of R1T. **B**. Homologous competition of 13 nM [^{3}H]EB and α4β2 nAChR. Compared with A, the larger [^{3}H]EB concentration leads to an initially larger IC_{50} at small R1T (Eq. (13)) and a larger R1T concentration needed for the onset of significant ligand depletion. The curves for the five smallest R1T values overlap and form the leftmost solid curve. The competition curves of both A and B are distorted away from sigmoidal shape as ligand depletion increases.

results showed that increasing ligand depletion in homologous competition data shifted IC_{50} rightward and caused asymmetric curves around IC_{50}.

As ligand depletion increased, its effect on binding to the high affinity site became qualitatively different from its effect on binding to the low affinity site. With negligible ligand depletion at R1T = 0.00013 nM and [^{3}H]EB = 0.013 nM, homologous competition of [^{3}H]EB binding to the high and low affinity sites produced similarly shaped sigmoidal competition curves (Figure 8A and 8B). With substantial ligand depletion at R1T = 130 nM and [^{3}H]EB = 0.013 nM, [^{3}H]EB binding to the high affinity site acquired a sharp shoulder but continued to decrease monotonically with increasing cold EB (Figure 8C). At the low affinity site, substantial ligand depletion produced an asymmetric peak of [^{3}H]EB binding (Figure 8D).

Characterizing the low-affinity specific binding site with homologous competition when NSB is negligible

How well can homologous competition data with ligand depletion identify the low affinity binding site? Comparing fits from the one site model$_{total}$ and two sites model$_{total}$ to noisy data from a single [^{3}H]EB concentration reliably achieved this goal only with highly precise data (maximum S/N = 1000) (Figure 9A). With 20 nM [^{3}H]EB, [^{3}H]EB occupied a large fraction (62%) of the low affinity binding site when cold EB was absent. The result with 20 nM [^{3}H]EB and 0.13 nM R1T suggested that occupying both high and low affinity sites using one high [^{3}H]EB concentration was insufficient to identify the low affinity site when S/N values were realistic. Figure 8C and 8D, however, suggested that combining concentrations of [^{3}H]EB and binding sites on the order of K_{d2} might lead to a distinctive concentration dependence of [^{3}H]EB binding that would identify the low affinity binding site with less precise data. Indeed, concentrations of 20 nM [^{3}H]EB and 20 nM R1T reliably achieved this goal with less precise data (maximum S/N = 50) (Figure 9A). These results suggested that homologous competition data from a single [^{3}H]EB concentration could identify the low affinity binding site with realistically precise data using large concentrations of [^{3}H]EB and α4β2 nAChR binding sites. This approach, however, consumed large amounts of [^{3}H]EB and α4β2 nAChR.

Multiple concentrations of [^{3}H]EB that explored a wide range of fractional occupancies of the two binding sites might identify the low affinity binding site while consuming less [^{3}H]EB and α4β2 nAChR. Improving the interpretation of homologous competition data from two binding sites by using several concentrations of radioligand has been described for a general case [7]. To test this method with [^{3}H]EB and α4β2 nAChR, homologous competition data sets from [^{3}H]EB concentrations of 0.013, 0.3, and 20 nM and R1T = 0.13 nM were generated (Figure 9B-E). Multiple concentrations of [^{3}H]EB required less precise data and consumed less [^{3}H]EB and α4β2 nAChR to identify the low affinity site than did a single large [^{3}H]EB concentration (Figure 9A).

Characterizing the low-affinity specific binding site with homologous competition when NSB is significant

In practice, NSB is not zero and needs to be included in a model of homologous competition data. NSB, as expected, moved the baseline above zero at large concentrations of cold EB. Increasing ligand depletion shifted IC_{50} rightward and distorted the monotonically decreasing sigmoidal shape of the competition curve (Figure 10A). As expected from modeling of one specific binding site [19], the contribution of NSB to total [^{3}H]EB binding across the range of cold EB concentration depended on the extent of ligand depletion (Figure 10B). The dependence of NSB on ligand

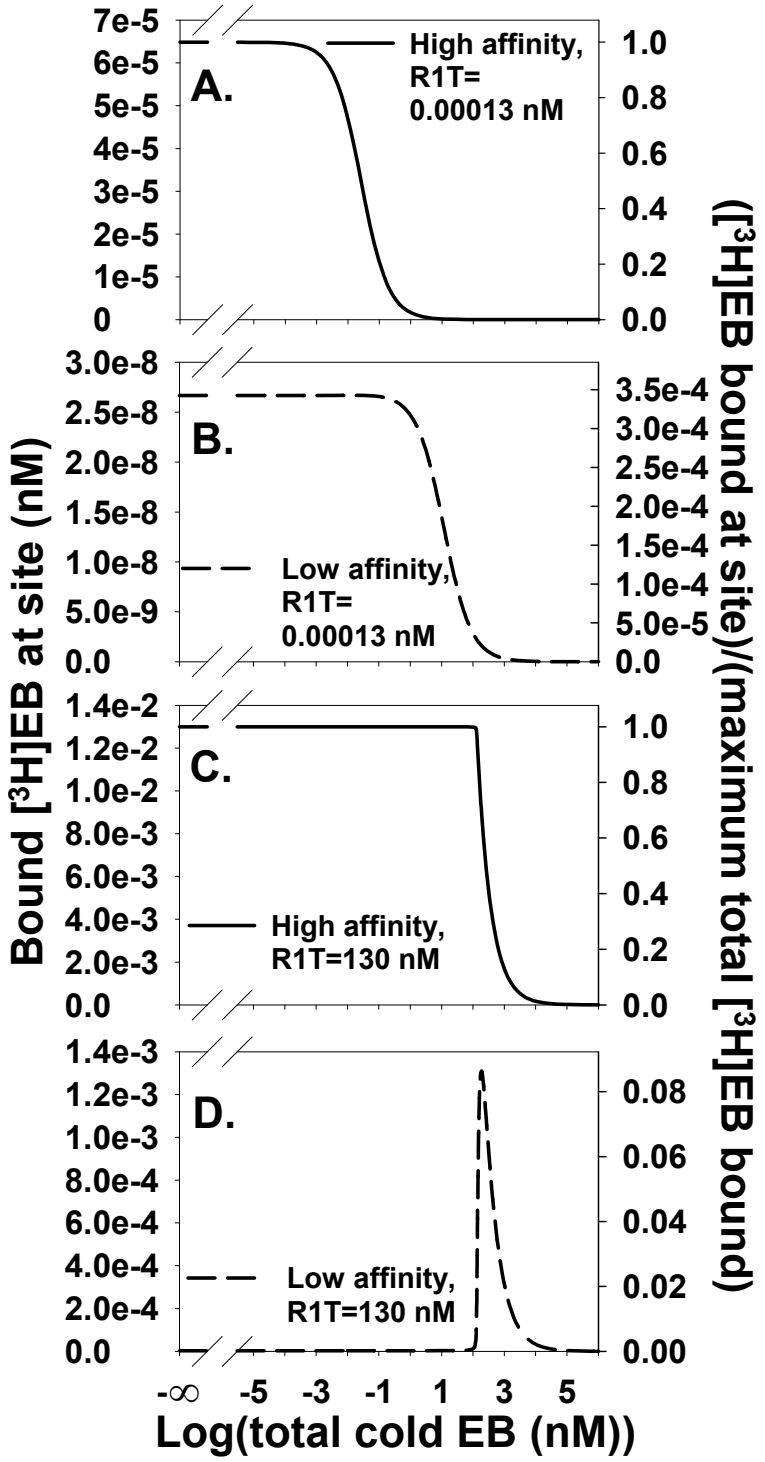

Figure 8 Homologous competition of [^{3}H]EB at the low affinity site is substantially different from competition at the high affinity site when ligand depletion is significant. **A** and **B**. Homologous competition from the high affinity site (A) and the low affinity site (B) with [^{3}H]EB = 0.013 nM and R1T = 0.00013 nM leads to negligible depletion of [^{3}H]EB. The competition curves are sigmoidal. **C** and **D**. [^{3}H]EB = 0.013 nM and R1T = 130 nM lead to significant ligand depletion. Competition at the high affinity site (C) with ligand depletion is a distorted sigmoid curve similar to the total competition curves at high ligand depletion in Figure 7. In contrast, competition at the low affinity site (D) is a peak with maximum binding at 190 nM cold EB. From the right-hand scales of A and B with the right-hand scales of C and D, ligand depletion changes the fractional contribution of the low affinity site to the total binding. The low affinity site contributes less than 3.5×10^{-4} of the maximum total binding when ligand depletion is negligible (A and B). In contrast, the low affinity site contributes more than 0.08 of the maximum total binding with significant ligand depletion (C and D).

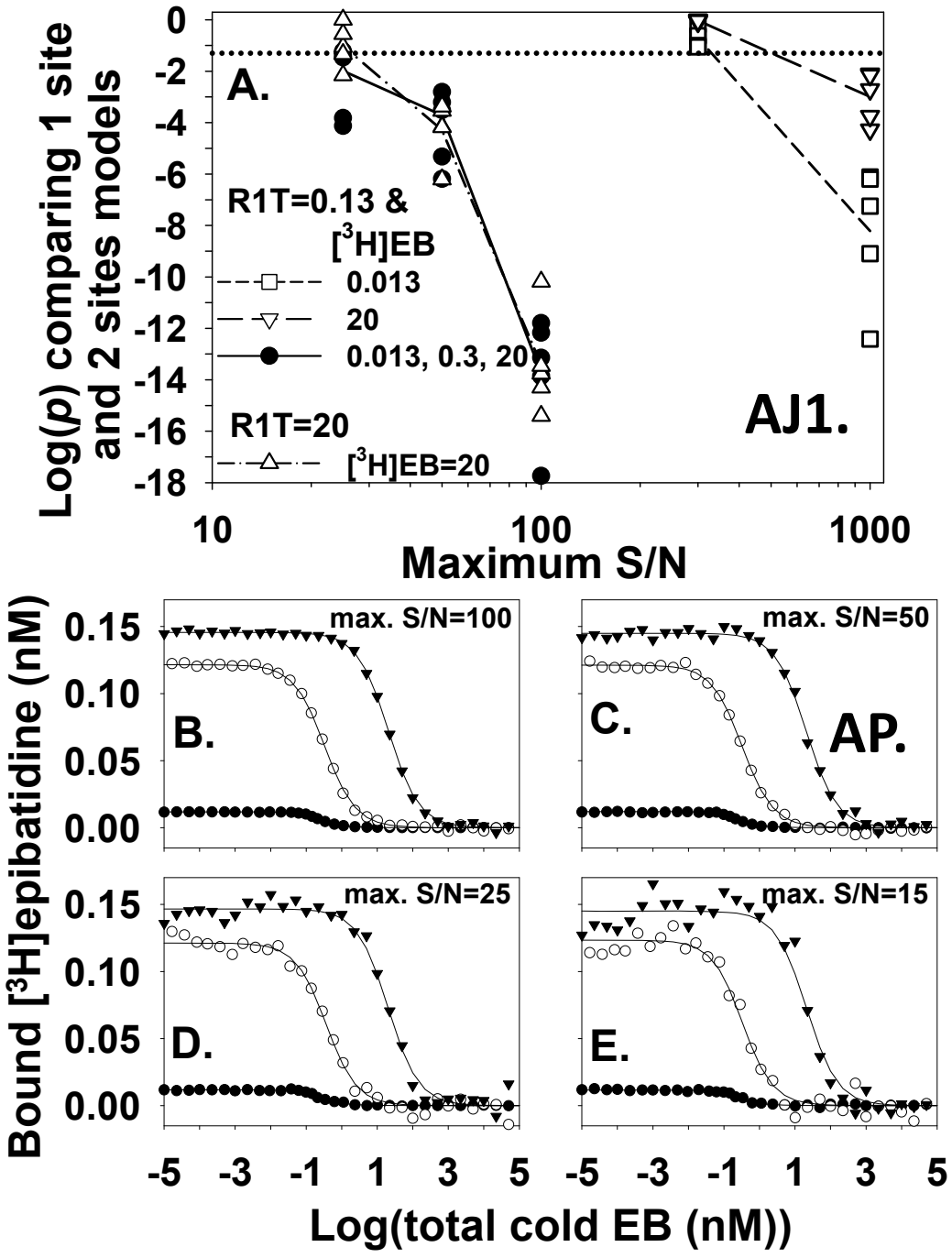

Figure 9 Data exploring a wide range of fractional occupancies of both binding sites help identify the low affinity binding site with homologous competition data with zero NSB. **A**. The *p*-values comparing one site model$_{total}$ and two sites model$_{total}$ depend on the maximum S/N in the homologous competition data. With R1T = 0.13 nM, single concentrations of [^{3}H]EB with ([^{3}H]EB = 0.013 nM; □; average log(*p*), short dashed line) or without ([^{3}H]EB = 20 nM;∇; average log(*p*), long dashed line) ligand depletion require highly precise data (maximum S/N > 300) to consistently achieve $p < 0.05$ ($p = 0.05$, dotted line). When [^{3}H]EB and R1T are 20 nM (Δ; average log(*p*), dash-dot line) and ligand depletion is significant, less precise data are needed to consistently achieve $p < 0.05$. With the same number of data points (114 points), simultaneous fitting of data from concentrations of [^{3}H]EB at 0.013, 0.3, and 20 nM with R1T = 0.13 nM (●; average log(*p*), solid line) also needs less precise data to consistently achieve $p < 0.05$. Number of trials at each concentration and S/N value was 5. Estimates of dissociation constants and binding site concentrations are not significantly different from true values when S/N = 50. The CIs of K_{d1} (9.6 - 13.8 pM; mean = 11.5 pM) and K_{d2} (1.9-22.0 nM; mean = 6.5 nM) and CIs of R1T (0.126-0.131; mean = 0.128) and R2T (0.0198-0.0315; mean = 0.0256) ($n = 5$ for each CI) included the true values. **B**, **C**, **D**, and **E**. The two sites model$_{free}$ generated noisy homologous competition data sets with R1T = 0.13 nM; [^{3}H]EB = 0.013 (●), 0.3 (○), and 20 nM (▼); and maximum S/N = 100 (B), 50 (C), 25 (D), and 15 (E). Fitting the one site model$_{total}$ and two sites model$_{total}$ to these types of data sets produced *p* values in A. Lines shown are fits of two sites model$_{total}$.

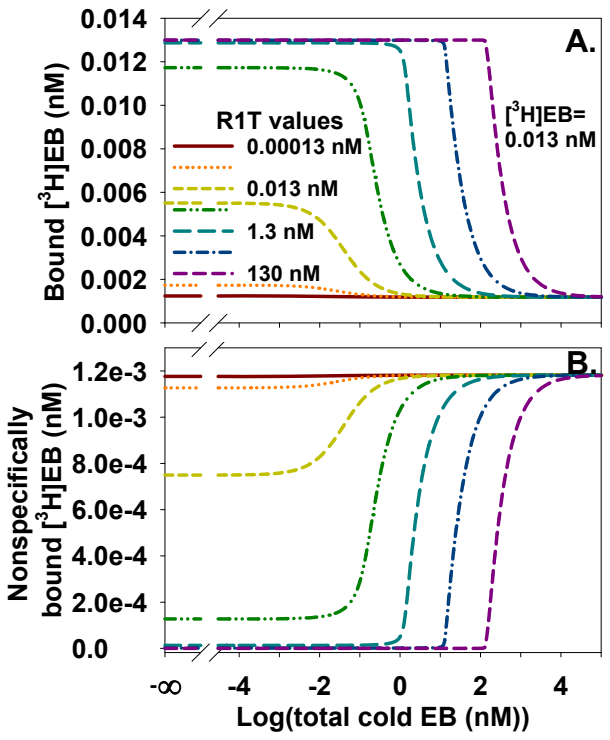

Figure 10 The contribution of NSB to total binding of homologous competition data depends on the concentration of cold EB when ligand depletion is significant. **A**. The presence of NSB (α = 0.1, [^{3}H]EB = 0.013 nM) displaces the baseline of bound [^{3}H]EB above the *x*-axis. Ligand depletion does not affect the size of this signal at large concentrations of cold EB, which in this case is equivalent to the apparent NSB. As anticipated from Figure 7, increasing ligand depletion in the presence of NSB shifts IC_{50} rightward and distorts the sigmoidal shape of the competition curve. R1T values increase in one log unit increments. **B**. NSB is not constant along the *x*-axis. Increasing ligand depletion with increasing R1T reveals the sigmoidal or distorted sigmoidal appearance of NSB as a function of cold EB and shifts the NSB curve rightward. Conditions and legend are the same as in A.

depletion showed that simply subtracting the baseline of bound [^{3}H]EB at large cold EB concentration from total bound [^{3}H]EB did not accurately calculate specifically bound [^{3}H]EB. Instead, and similar to saturation binding with ligand depletion and NSB, interpreting properties of specific binding of homologous competition data with NSB needed fitting of total binding.

Homologous competition without NSB suggested simultaneously fitting data from several [^{3}H]EB concentrations at a constant concentration of $\alpha4\beta2$ nAChR better identified the low affinity site than did fitting data from a single [^{3}H]EB concentration (Figure 9A). Applying this approach at 0.013, 0.3, and 20 nM [^{3}H]EB to homologous competition with R1T = 0.13 nM and α = 0.1, however, revealed that NSB overwhelmed specific binding at 20 nM [^{3}H]EB. 92% of total [^{3}H]EB binding was NSB, 7% was bound to the high affinity site, and only 1% was bound to the low affinity site in the absence of cold EB.

As suggested by Figures 8 and 9A, concentrations of both [^{3}H]EB and R1T on the order of K_{d2} might help identify binding to the low affinity site. This method populates the low affinity site relative to the high affinity site and to NSB (Figure 11A). This method with [^{3}H]EB and R1T at 20 nM identified binding to the low affinity site with five of five data sets at S/N = 50 and three of five data sets at S/N = 25 (Figure 11B). The consumption of a large concentration of [^{3}H]EB and $\alpha4\beta2$ nAChR at all data points, however, was an undesirable outcome.

To reduce [^{3}H]EB and $\alpha4\beta2$ nAChR consumption, both binding sites and [^{3}H]EB were varied. This method could sample a wide range of fractional occupancies of the two binding sites, which suggested a potential advantage for interpreting binding to the specific sites (Figure 11A). The maximum fractional occupancies (R1L/R1T) of the high affinity site by [^{3}H]EB were 0.089, 0.29, and 0.97 at [^{3}]EB = 0.013, 0.3, and 20 nM and at R1T = 0.13, 1, and 20 nM. For the low affinity site, the maximum fractional occupancies (R2L/R2T) were 0.00081, 0.014, and 0.29. NSB made a greater fractional contribution to total binding than the low affinity site for all concentrations of cold EB when [^{3}H]EB = 0.013 nM and R1T = 0.13 nM. With [^{3}H]EB and R1T at 20 nM, however, [^{3}H]EB binding by the low affinity site was greater than NSB up to 24 nM cold EB (Figure 11A). These results suggested this method might adequately sample the contribution by the low affinity site to total binding during fitting of noisy data when NSB was significant.

The method was tested by comparing one site model$_{total}$ and two sites model$_{total}$ fits to noisy data from three pairs of [^{3}H]EB concentrations and binding site concentrations. The low affinity site was identified with five of five data sets with S/N = 50 and four of five data sets with S/N = 25 (Figure 11B). These results suggested that simultaneous fitting of homologous competition data from several concentrations of [^{3}H]EB and binding sites has the potential to identify low-affinity specific binding in the presence of NSB.

Potential misinterpretation of low-affinity specific binding as NSB in homologous competition binding

Even with highly precise data, Eqs. (3) to (5) suggested a possibility of misinterpreting low-affinity specific binding as NSB in homologous competition data when only fitting total binding data. A low affinity, second specific binding site with a large relative concentration could mimic NSB as long as R2≈R2T over the range of cold EB concentration. Although a large relative concentration of the second binding site was not observed from expression of $\alpha4\beta2$ nAChR in oocytes [18], such a condition potentially could arise in a different heterologous

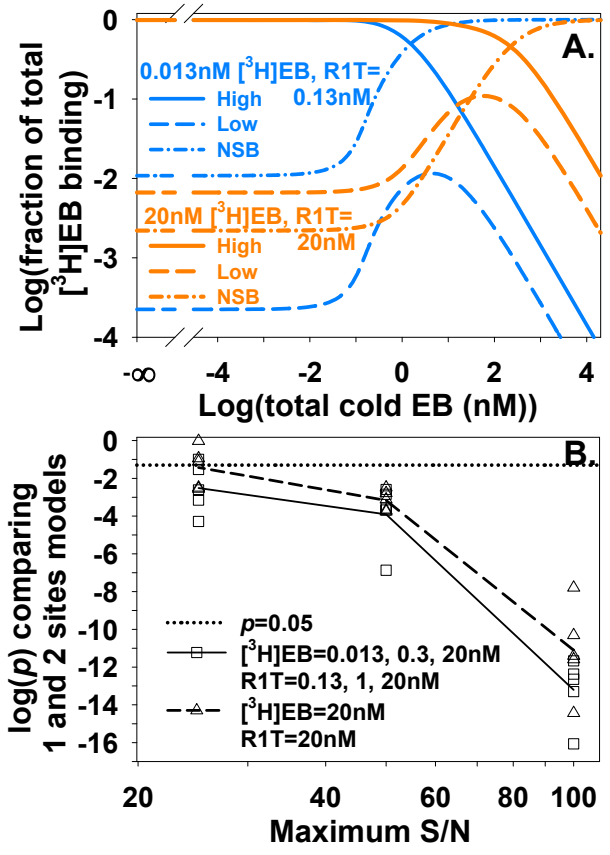

Figure 11 Ligand depletion helps identify the low affinity site when NSB is significant in competition data. **A**. Increasing concentrations of binding sites and [^{3}H]EB samples a wide range of fractional contributions of the two binding sites and NSB to total binding. The combination [^{3}H]EB = 0.013 nM and R1T = 0.13 nM mostly samples behavior of the high affinity site. The low affinity site contributes at most one-hundredth of the total binding; its contribution is always smaller than NSB. In contrast, the combination [^{3}H]EB = 20 nM and R1T = 20 nM more effectively samples behavior of the low affinity site. The low affinity site contributes a maximum of one-tenth of the total binding and contributes more than NSB does to total binding up to about 20 nM cold EB. The *y*-axis values are calculated as *Q*/(R1L+R2L+NSB) where *Q* = R1L, R2L, or NSB. These results suggest this approach might adequately sample the contribution from the low affinity site to total binding during fitting of noisy data. **B**. The *p* values compare fits from one site model$_{total}$ and two sites model$_{total}$ to competition data generated with α = 0.1. One set (Δ) used [^{3}H]EB = R1T = 20 nM; the second set (□), [^{3}H]EB = 0.013, 0.3, and 20 nM and R1T = 0.13, 1, and 20 nM. Lines show average log(*p*). At S/N = 50 for the first set, CIs included the true values (K_{d1} = 0.016 nM (CI: 0.010-0.025 nM); K_{d2} = 14.9 nM (CI: 6.3-35 nM); R1T = 20.2 nM (CI: 19.7-20.6 nM); R2T = 4.7 nM (CI: 2.8-6.6 nM); α = 0.096 (CI: 0.091-0.100) (*n* = 5 for each CI). At S/N = 25 for the second set, CIs included the true values (K_{d1} = 0.012 nM (CI: 0.009-0.014 nM); K_{d2} = 17.0 nM (CI: 4.3-66 nM); fraction of R2T = 0.28 (CI: 0.11-0.45); α = 0.10 (CI: 0.093-0.108).

expression system. The potential for confusing low-affinity specific binding and NSB was explored by comparing homologous competition data from a one site model$_{free}$ with α = 0.2 with data from a two sites model$_{free}$ with α = 0 and K_{d2} = R2T/0.2. As R2T and K_{d2} increased, the upper limit of cold EB concentration for which R2 R2T remained valid also increased. The data from the two sites model$_{free}$ with zero NSB, therefore, displayed increasingly long plateaus mimicking NSB at large concentrations of cold EB. The long plateaus, however, arose from specific binding to the low affinity α4β2 nAChR binding site and not from NSB. Figure 12A suggested that homologous competition data at a single [^{3}H]EB concentration might not distinguish binding to a low affinity site from NSB unless either the maximum concentration of cold EB exceeded K_{d2} or NSB was measured without α4β2 nAChR.

Heterologous competition with ligand depletion and NSB

Homologous competition is a specific case of the more general case of heterologous competition, for which the dissociation constants of the radioligand and the heterologous competitor differ. For heterologous competition, identification of a low affinity site and estimates for dissociation constants for [^{3}H]EB to high and low affinity sites typically are determined from saturation binding. In this case, inhibition constants (K_{i1} and K_{i2} in Figure 1) for the competitor and the concentration of binding sites are the only unknowns when fitting heterologous displacement data. This study focuses on how ligand depletion and NSB affects heterologous competition with high and low affinity binding sites of [^{3}H]EB. In addition, this study investigates concentrations of [^{3}H]EB and α4β2 nAChR that might facilitate studying the low affinity site.

To determine how ligand depletion without NSB affects heterologous competition with [^{3}H]EB and α4β2 nAChR, competition data at increasing concentrations of binding sites were generated with nicotine as the competitor. The dissociation constants for nicotine were 0.84 nM for the high affinity site [18] and 775 nM for the low affinity site. The inhibition constant for nicotine at the low affinity site was assigned so that K_{i2}/K_{i1} for nicotine = K_{d2}/K_{d1} for EB. When ligand depletion was negligible, IC_{50} values varied only slightly with binding site concentration (Figure 13A-F). The K_i values derived from these IC_{50} values and the Cheng-Prusoff equation (Eq. (14)),

$$IC_{50} = [^3\text{H}]\text{epibatidine} + K_i \quad (14)$$

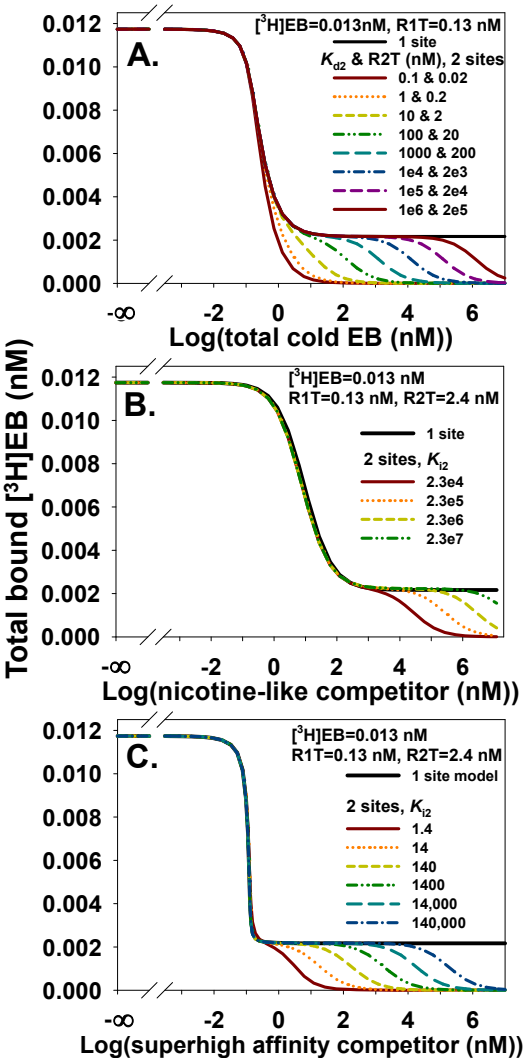

Figure 12 Binding to a low affinity second binding site with hypothetically large R2T and K_{d2} or K_{i2} values mimic NSB in homologous and heterologous competition data. **A**. The one site model$_{free}$ (α = 0.2) and two sites model$_{free}$ (α = 0) generated homologous competition data with K_{d2} = R2T/0.2. With increasing R2T and K_{d2}, the two sites model$_{free}$ produces increasingly long plateaus of total bound [^{3}H]EB, similar to NSB. Low-affinity specific binding is distinguished from NSB only when cold EB concentration exceeds K_{d2}. **B**. Heterologous competition of [^{3}H]EB with a nicotine-like competitor at a low affinity site can mimic NSB. The one site model$_{free}$ with α = 0.2 generated heterologous competition data with K_{i1} = 0.84 nM for the competitor (value for nicotine [18]). With these values and R2T = 2.4 nM and α = 0, the two sites model$_{total}$ fits these data well up to a competitor concentration of K_{i2}. Low-affinity specific binding is distinguished from NSB only when the competitor concentration exceeds K_{i2}. **C**. With a superhigh affinity competitor, increasing R2T and varying K_{i2} with heterologous competition of [^{3}H]EB at a low affinity site can mimic NSB. The one site model$_{free}$ with α = 0.2 generated heterologous competition data with $K_{i1} = 1.3 \times 10^{-4}$ nM. With α = 0, the two sites model$_{total}$ fits well to these data up to a competitor concentration of K_{i2}. Low-affinity specific binding is distinguished from NSB only when competitor concentration exceeds K_{i2}.

which assumes a single binding site without ligand depletion, were close to K_{i1} for nicotine (0.90, 0.87, and 0.96 nM at 0.013, 0.3, and 20 nM [^{3}H]EB and R1T = 0.00013 nM). As increasing ligand depletion shifted IC_{50} rightward (Figure 13A-F), the estimate of K_i from the Cheng-Prusoff equation no longer closely matched K_{i1} for nicotine. The shape of the competition curve remained approximately sigmoidal with a Hill coefficient consistently near -1 at all levels of ligand depletion.

Although nicotine binds more weakly than [^{3}H]EB to $\alpha4\beta2$ nAChR, other ligands developed in the future, especially derivatives of EB, conceivably might bind more tightly than [^{3}H]EB. To determine how ligand depletion affects heterologous competition with a superhigh affinity competitor, heterologous competition data were generated with two dissociation constants 100-fold tighter (1.3×10^{-4} and 0.12 nM) than the two dissociation constants for [^{3}H]EB. When ligand depletion of [^{3}H]EB was negligible, IC_{50} values were independent of binding site concentration and led to slightly high estimates of K_{i1} (1.4×10^{-4} nM) using Eq. (14); Hill coefficients were about -1 (Figure 13G-L). Increasing ligand depletion shifted IC_{50} rightward and, in contrast to nicotine, shifted Hill coefficients to strongly negative values (for example, -35 with [^{3}H]EB = 0.013 nM and R1T = 130 nM). These results showed the effect of ligand depletion on the Hill coefficient depended markedly on whether the competitor bound more tightly or less tightly than [^{3}H]EB.

K_{i2} for a competitor potentially can be estimated with procedures analogous to procedures investigated for homologous competition. To test the approach described in Figures 9 and 11 for homologous competition, noisy heterologous competition data for nicotine and [^{3}H]EB with ligand depletion and NSB were fit with the two sites$_{total}$ model (Figure 14). A single 0.013 nM concentration of [^{3}H]EB with R1T = 0.13 nM did not significantly populate the low affinity site (Figure 14A). That concentration combination produced reliable estimates of K_{i2} only with highly precise data (maximum S/N ≥ 1000) (Figure 14C). At maximum S/N = 100, fits with competition by nicotine at the high and low affinity sites generally were not significantly better than fits with competition by nicotine at only the high affinity site (p > 0.05 for six of six trials). Similar to the findings in Figures 9 and 11, increasing ligand depletion and populating both the high and low affinity sites with larger concentrations of [^{3}H]EB and $\alpha4\beta2$ nAChR (Figure 14B) allowed more reliable estimates of K_{i2} with less precise data (Figure 14C). At maximum S/N = 15 with this approach, fits with competition by nicotine at the two [^{3}H]EB binding sites generally were significantly better than fits with competition by nicotine at only the high affinity site ($0.007 < p < 5 \times 10^{-10}$ for six of six trials). These results

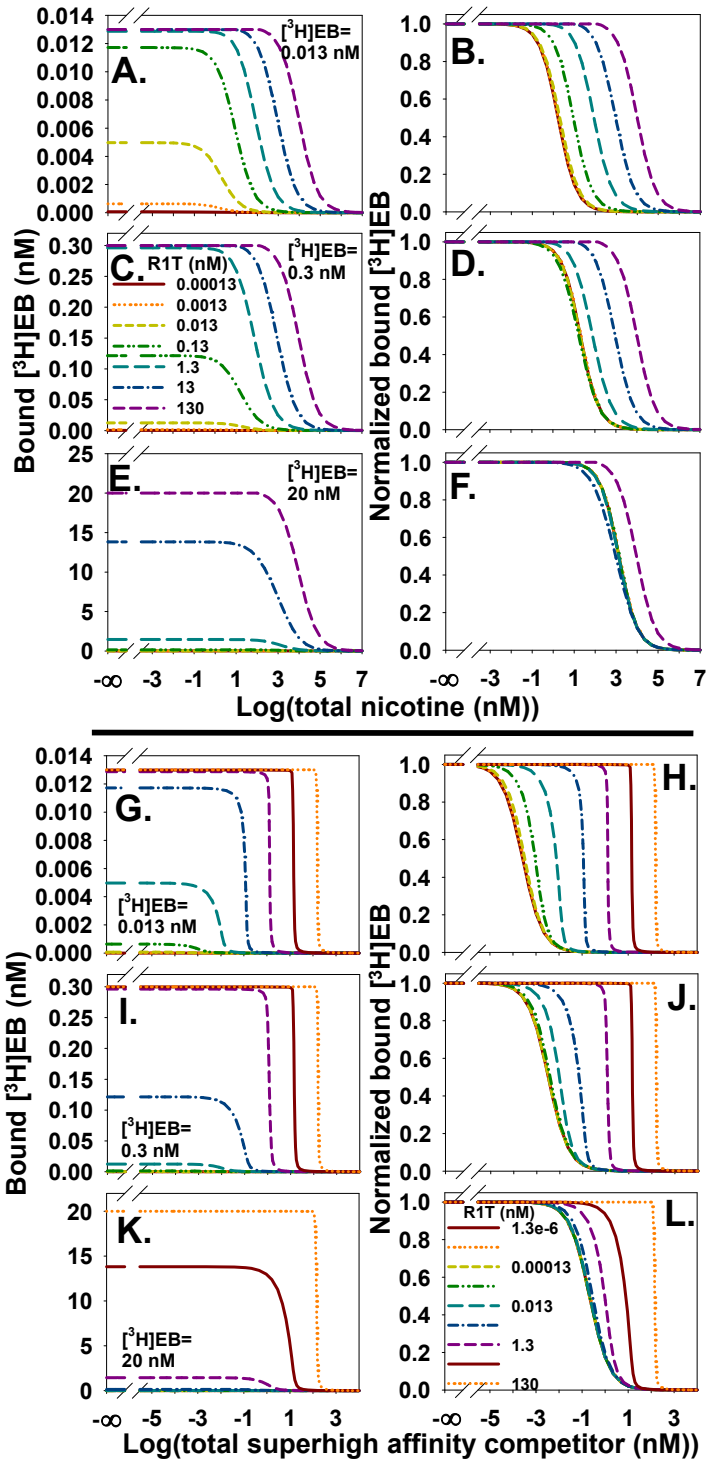

Figure 13 Effects of ligand depletion on heterologous competition data depend on the relative affinity of the inhibitor. **A-F**. Competition data for [^{3}H]EB and nicotine were generated with two sites model$_{free}$ with [^{3}H]EB = 0.013 (A & B), 0.3 (C & D), and 20 nM (E & F) and the R1T values shown in C. The *y*-axes of A, C, and E show total bound [^{3}H]EB; *y*-axes of B, D, and F show normalized binding for comparing IC_{50} values. Data from small values of R1T are not distinguishable because of the ranges of the *y*-axis scales (A, C, and E) or because data sets overlap when rightward shifts of IC_{50} are negligible (B, D, and F). Ligand depletion shifts IC_{50} rightward; shape of the competition curve remains approximately sigmoidal. **G-L**. Competition data for [^{3}H]EB and a hypothetical superhigh affinity competitor were generated with two sites model$_{free}$ with [^{3}H]EB = 0.013 (G & H), 0.3 (I & J), and 20 nM (K & L) and the R1T values shown in L. The two inhibition constants K_{i1} and K_{i2} were 100-fold tighter (1.3×10^{-4} and 0.12 nM) than K_{d1} and K_{d2} for [^{3}H]EB. Ligand depletion shifts IC_{50} rightward and increases the maximum steepness of the negative slope of the sigmoidal shape. Hill coefficients at R1T = 130 nM are -35, -35, and -17 for [^{3}H]EB = 0.013, 0.3, and 20 nM.

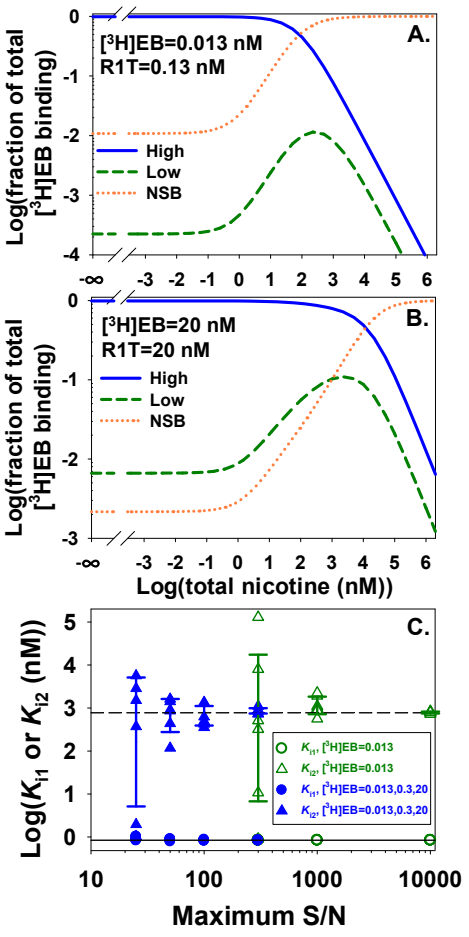

Figure 14 Ligand depletion improves precision of estimated K_{i2} for nicotine with noisy data and NSB. Ligand depletion improves precision of estimated K_{i2} for nicotine with noisy data. **A** and **B**. Increasing concentrations of binding sites and [^{3}H]EB samples a wide range of fractional contributions of the two binding sites and NSB to total [^{3}H]EB binding as nicotine concentration varies. In A, the combination [^{3}H]EB = 0.013 nM and R1T = 0.13 nM predominantly samples interaction between [^{3}H]EB and nicotine at the high affinity site. In B, the combination [^{3}H]EB = 20 nM and R1T = 20 nM with substantial ligand depletion more effectively samples interaction between [^{3}H]EB and nicotine at the low affinity site. The low affinity site contributes a maximum of one-tenth of total [^{3}H]EB binding and contributes more than NSB does to total [^{3}H]EB binding up to about 1000 nM nicotine. The *y*-axis values were calculated as Q/(R1L+R2L+NSB) where *Q* = R1L, R2L, or NSB. **C**. Noisy heterologous competition data for [^{3}H]EB and nicotine with various maximum S/N were fit with two sites$_{total}$ model to estimate K_{i1} and K_{i2}. The K_{i2} estimates shown with green Δ were derived with R1T = 0.13 nM. Modest ligand depletion and negligible occupancy by [^{3}H]EB of the low affinity binding site lead to low precision of K_{i2} estimates at maximum S/N = 300. K_{i2} estimates shown with blue ▲ were derived with R1T = 0.13, 1, 20 nM. Increasing ligand depletion and occupancy of the low affinity site by [^{3}H]EB lead to more precise K_{i2} estimates with noisier data. Error bars show standard deviations. K_{i1} estimates (green ○ or blue ●) are relatively independent of maximum S/N values. The number of data points (114 points) was identical in the two sets of estimates. Solid line: true K_{i1} (0.84 nM); dashed line: true K_{i2} (775 nM); α_L = 0.1; α_B = 0.

suggest that fitting data with large ligand depletion might identify the presence of nicotine competition at the low affinity site even if those data have a low S/N and an estimate of K_{i2} has low precision.

Similar to homologous competition data (Figure 12A), low-affinity specific binding might be misinterpreted as NSB when fitting heterologous competition data with a model of total binding. To investigate this possibility with a nicotine-like inhibitor (K_{i1} = 0.84 nM), heterologous depletion data from the one site model$_{free}$ with NSB (α = 0.2) were compared to data from the two sites model$_{total}$ without NSB. With R2T = 2.4 nM and various values of K_{i2}, the two sites model$_{total}$ produced a long plateau mimicking NSB (Figure 12B). The value of K_{i2} at this constant value of R2T determined the length of the plateau along the *x*-axis. One log unit increase of the value of K_{i2} lengthened the plateau of binding to the low affinity site by one log unit. A competitor binding more tightly than [^{3}H]EB to the high affinity binding site produced similar results (Figure 12C). These results suggested that binding to the low affinity site might be identified as NSB at a single [^{3}H]EB concentration unless either the maximum competitor concentration was greater than K_{i2} or NSB was measured without α4β2 nAChR.

Characterizing high and low affinity binding sites when NSB of a heterologous competitor is unknown

The NSB of an unlabeled competitor is not measured by heterologous competition measurements and often is assumed to be zero. The true value of $\alpha_{competitor}$, therefore, presents a source of uncertainty about values of inhibition constants. This uncertainty was investigated by increasing values of $\alpha_{competitor}$ while nicotine (Figure 15A) or a superhigh affinity competitor (Figure 15C) inhibited binding of [^{3}H]EB to α4β2 nAChR. As the true value of $\alpha_{competitor}$ for nicotine increased, apparent values of K_{i1} ($K_{i1,\ app}$) and K_{i2} ($K_{i2,\ app}$) also increased (Figure 15B). The contours of competition curves with the superhigh affinity competitor changed as $\alpha_{competitor}$ increased (Figure 15C), in contrast to the constant contours with nicotine. The ratio $K_{i2,\ app}/K_{i1,\ app}$ for the superhigh affinity competitor, however, was invariant as $\alpha_{competitor}$ increased (Figure 15D). The invariance of $K_{i2,\ app}/K_{i1,\ app}$ at the two binding sites of α4β2 nAChR is important because the ratio represents the difference in free energy of binding at the two binding sites. This difference reflects differences in the interactions between the competitor and binding sites and structural differences between the high and low affinity binding sites. This measured free energy difference is independent of $\alpha_{competitor}$.

Discussion

A model that fits total binding data as a function of total ligand can correctly interpret those data when

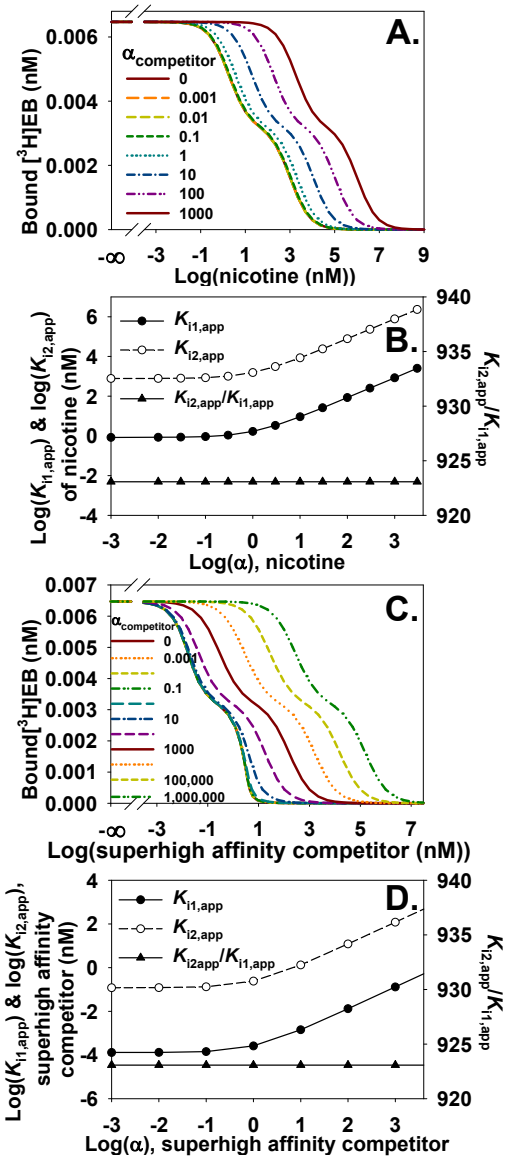

Figure 15 NSB of a competitor changes $K_{i1,\ app}$ and $K_{i2,\ app}$ but not $K_{i2,\ app}/K_{i1,\ app}$. **A**. The two sites model$_{free}$ generated competition data for [^{3}H]EB and nicotine with R1T = 0.013 nM and R2T = 3.9 nM so the competition curve clearly shows the two binding sites. Increasing $\alpha_{competitor}$ shifted the curve rightward without changing the shape of the curve. **B**. To determine how increasing $\alpha_{competitor}$ affected apparent values of K_{i1} ($K_{i1,\ app}$) and K_{i2} ($K_{i2,\ app}$) with $\alpha_{competitor,\ app}$ = 0, two sites model$_{total}$ was fitted to the competition curves in A. The only degrees of freedom for this fitting were $K_{i1,\ app}$ and $K_{i2,\ app}$ for nicotine. Increasing $\alpha_{competitor}$ increases $K_{i1,\ app}$ and $K_{i2,\ app}$ but does not change $K_{i2,\ app}/K_{i1,\ app}$, a ratio reflecting the difference in free energy of nicotine binding at the two sites. **C**. Similar to A, the two sites model$_{free}$ generated competition data for [^{3}H]EB and a superhigh affinity competitor with R1T = 0.013 nM, R2T = 3.9 nM, K_{i1} = 0.00013 nM, and K_{i2} = 0.12 nM. The curves clearly show the two binding sites. In contrast to A, shapes of the competition curves change as increasing $\alpha_{competitor}$ shifts the curve rightward. **D**. Similar to nicotine, $K_{i2,\ app}/K_{i1,\ app}$ for the superhigh affinity competitor does not vary with $\alpha_{competitor}$.

ligand depletion and NSB are significant [19]. This approach is straightforward with one binding site. This study shows that the approach for [^{3}H]EB, α4β2 nAChR, and two binding sites needs modifications for identifying binding to the low affinity site. In particular, identifying the low affinity site can be challenging because of phenomenological and computational similarities between low-affinity specific binding and NSB.

This study is novel because it shows that fitting total binding data from [^{3}H]EB and α4β2 nAChR might be insufficient for characterizing the low affinity site when ligand depletion and NSB are significant. Moreover, this investigation develops four concepts for studying the low affinity binding site of α4β2 nAChR in the presence of ligand depletion and NSB that go beyond simply fitting total binding. First, binding of [^{3}H]EB to the low affinity site in saturation data or homologous competition data can be misattributed to NSB. Low-affinity specific binding can be identified by using larger maximum concentrations of [^{3}H]EB or cold competitor, simultaneously fitting apparent NSB, or obtaining data from multiple concentrations of α4β2 nAChR. Potential ambiguity between low-affinity specific binding and NSB arises because they share a similar appearance as long as R2≃R2T. Increasing [^{3}H]EB$_{max}$ for saturation binding or increasing the maximum concentration of cold competitor for competition binding breaks this similarity by creating conditions for which R2≪R2T, R2L≃R2T, and R2B≃R2T.

Second, when NSB is significant, ligand depletion can help characterize the low affinity site. Ligand depletion in binding studies is commonly believed to be only problematic. In contrast, increasing ligand depletion by increasing α4β2 nAChR concentration beneficially reduced NSB and significantly populated the low affinity site. The result was better detection of [^{3}H]EB binding to the low affinity site.

Third, directly measuring NSB without α4β2 nAChR can more reliably interpret NSB than does modeling NSB as a component of total binding in competition binding. Whether [^{3}H]EB binding at a particular large concentration of competitor arises solely from NSB depends on K_{i2} and concentration of the low affinity site. Removing α4β2 nAChR from the assay, when feasible, is a more rigorous way than is using a large concentration of competitor to ensure that [^{3}H]EB binding arises from NSB and does not involve the low affinity site of α4β2 nAChR.

Fourth, $\alpha_{competitor}$ needs to be considered when interpreting heterologous competition data with [^{3}H]EB and α4β2 nAChR because it increases $K_{i1,\ app}$ and $K_{i2,\ app}$. The true values of K_{i1} and K_{i2}, therefore, can be determined only when $\alpha_{competitor}$ is known. Regardless of $\alpha_{competitor}$, however, $K_{i2,\ app}/K_{i1,\ app}$ is invariant and

equals K_{i2}/K_{i1}. This ratio can help compare structural features of the two binding sites of α4β2 nAChR. For example, variations in the ratio for a series of competitors with systematic structural variations might correlate with structural features of the two binding sites.

The findings presented in this study have limitations. First, modeling explored conditions suitable for characterizing low affinity binding that might not match conditions readily available in a laboratory. One such condition is nanomolar concentrations of α4β2 nAChR. This high range of α4β2 nAChR concentration might be more available in the future with high level heterologous expression of α4β2 nAChR. Quantitative results, such as concentration ranges that identify the low affinity site, are a reasonable but not definitive guide to conditions for studying the low affinity site of α4β2 nAChR with [^{3}H]EB. For example, values of α might be substantially smaller than the values illustrating NSB in this study. With membrane homogenates from stably transfected HEK 293 cells, α was on the order of 0.001 [52]. In addition, changes in the fraction of low affinity site, as might occur with different expression conditions, will change the appearance of data. A larger fraction of low affinity site would make detection and analysis of this site easier. Second, the simulations included large numbers of data points with the goal of reliably describing binding data. Fewer data points would need higher precision in the data to identify the low affinity site and would lead to reduced precision of binding parameter estimates. Third, the properties of noise imposed on errorless data in this study do not necessarily reflect properties of real noise and uncertainties in experiments. Fourth, based on binding data from our laboratory [18], this study assumes two independent binding sites in α4β2 nAChR. Other descriptions of binding sites (for example, two cooperative binding sites, a combination of cooperative and independent binding sites, or more than two independent sites) might better describe binding data from α4β2 nAChR under other conditions. Fifth, the linear relationship between free [^{3}H]EB and NSB led to the phenomenological and computational similarity between low affinity binding and NSB expressed in Eqs. (3)-(5). This linear relationship usually describes the behavior of NSB. This linear relationship might be unsuitable for some situations. For example, if NSB in the absence of specific binding is observed to be saturable [53-55], the linear relationship would need to be modified. Sixth, statistical comparisons using the F-test and p values between the one site $\text{model}_{\text{total}}$ and two sites $\text{model}_{\text{total}}$ were suitable because of the nested nature of the two models. In other words, the two sites $\text{model}_{\text{total}}$ contained all the features of the one site $\text{model}_{\text{total}}$ and extended those features by a second specific binding site. Other statistical methods for comparing models do not need nested models, such as Akaike's information criterion [7,56,57]. Seventh, the independent variable for the models in this study is the concentration of total ligand ([^{3}H]EB for saturation binding or a cold ligand for competition). This variable usually is accurately known and was presumed to be free of uncertainty. Using the measured concentration of free ligand as the independent variable simplifies the model equations. The measured free ligand concentrations, however, will have nonnegligible uncertainty. The method of least squares might not reliably estimate parameter values when the values of the independent variable are uncertain [1,2,58].

Conclusions

Characterizing the low affinity site potentially will contribute understanding of structure, function, and synthesis of α4β2 nAChR in native and heterologous expression systems. For example, the low affinity site might arise from an immature form of α4β2 nAChR or be involved in ligand-induced upregulation [32,59-61]. Heterologous competition data similar to Figure 12B were found with cytisine, nicotine, and acetylcholine as competitors of [^{3}H]EB binding with α4β2 nAChR immunoisolated with monoclonal antibody (mAb) 295 but not with other mAbs [18]. This similarity suggests that mAb 295 might isolate a distinctive form of low affinity α4β2 nAChR. Homologous competition data might help further characterize this form of α4β2 nAChR. An intriguing possibility is that this low affinity form contributes to the biological roles of α4β2 nAChR. This study should help investigators design experiments and develop computational approaches for interpreting data from [^{3}H]EB and α4β2 nAChR when ligand depletion and NSB are significant. Manipulation of maximum ligand and receptor concentrations and intentionally increasing ligand depletion are potentially helpful approaches. Extending the modeling and numerical solution method to three or more binding sites and to cooperative binding with ligand depletion and NSB is straightforward. Although applied specifically to [^{3}H]EB and α4β2 nAChR, the methods should be relevant to other contexts of multiple binding sites, ligand depletion, and NSB.

Abbreviations

CI: 95% confidence interval; EB: epibatidine; mAb: monoclonal antibody; nAChR: nicotinic acetylcholine receptor; NSB: nonspecific binding; S/N: signal to noise ratio; SD: standard deviation; [^{3}H]EB: [^{3}H]epibatidine.

Acknowledgements

This study was financially supported by the Texas A&M University System Health Science Center.

Author details
[1]Department of Molecular and Cellular Medicine, Texas A&M University System Health Science Center, College Station, TX 77843-1114, USA. [2]Department of Neuroscience and Experimental Therapeutics, Texas A&M University System Health Science Center, Bryan, TX 77807-3260, USA. [3]Department of Veterinary Pathobiology, Texas A&M University, College Station, TX 77843-4467, USA.

Authors' contributions
AP determined the observed binding constants describing [^{3}H]epibatidine and nicotine binding to α4β2 nAChR and edited the manuscript. GW conceived the study, created the models, analyzed the simulations, and wrote the manuscript. Both authors read and approved the final manuscript.

Competing interests
The authors declare that they have no competing interests.

Received: 7 June 2011 Accepted: 23 November 2011
Published: 23 November 2011

References

1. Johnson ML: **The analysis of ligand-binding data with experimental uncertainties in the independent variables.** *Anal Biochem* 1985, **148**:471-478.
2. Tellinghuisen J: **The least-squares analysis of data from binding and enzyme kinetics studies: weights, bias, and confidence intervals in usual and unusual situations.** *Methods Enzymol* 2009, **467**:499-529.
3. Carter CM, Leighton-Davies JR, Charlton SJ: **Miniaturized receptor binding assays: complications arising from ligand depletion.** *J Biomol Screen* 2007, **12**:255-266.
4. Wells JW, Birdsall NJ, Burgen AS, Hulme EC: **Competitive binding studies with multiple sites. Effects arising from depletion of the free radioligand.** *Biochimica et biophysica acta* 1980, **632**:464-469.
5. Hulme EC, Birdsall NJM: **Strategy and tactics in receptor-binding studies.** In *Receptor-Ligand Interactions: A Practical Approach*. Edited by: Hulme EC. New York, NY: Oxford University Press; 1992:63-176, The Practical Approach Series.
6. Munson PJ, Rodbard D: **Ligand: a versatile computerized approach for characterization of ligand-binding systems.** *Anal Biochem* 1980, **107**:220-239.
7. Motulsky HJ, Christopoulos A: *Fitting models to biological data using linear and nonlinear regression. A practical guide to curve fitting* New York, NY: Oxford University Press; 2004.
8. Avlani VA, McLoughlin DJ, Sexton PM, Christopoulos A: **The impact of orthosteric radioligand depletion on the quantification of allosteric modulator interactions.** *J Pharmacol Exp Ther* 2008, **325**:927-934.
9. Wang ZX, Jiang RF: **A novel two-site binding equation presented in terms of the total ligand concentration.** *FEBS Lett* 1996, **392**:245-249.
10. Gnädisch D, London ED, Terry P, Hill GR, Mukhin AG: **High affinity binding of [^{3}H]epibatidine to rat brain membranes.** *Neuroreport* 1999, **10**:1631-1636.
11. Eaton JB, Peng JH, Schroeder KM, George AA, Fryer JD, Krishnan C, Buhlman L, Kuo YP, Steinlein O, Lukas RJ: **Characterization of human α4β2-nicotinic acetylcholine receptors stably and heterologously expressed in native nicotinic receptor-null SH-EP1 human epithelial cells.** *Mol Pharmacol* 2003, **64**:1283-1294.
12. Shafaee N, Houng M, Truong A, Viseshakul N, Figl A, Sandhu S, Forsayeth JR, Dwoskin LP, Crooks PA, Cohen BN: **Pharmacological similarities between native brain and heterologously expressed α4β2 nicotinic receptors.** *Br J Pharmacol* 1999, **128**:1291-1299.
13. Houghtling RA, Dávila-García MI, Hurt SD, Kellar KJ: **[^{3}H]Epibatidine binding to nicotinic cholinergic receptors in brain.** *Med Chem Res* 1994, **4**:538-546.
14. Truong A, Xing X, Forsayeth JR, Dwoskin LP, Crooks PA, Cohen BN: **Pharmacological differences between immunoisolated native brain and heterologously expressed rat α4β2 nicotinic receptors.** *Brain Res Mol Brain Res* 2001, **96**:68-76.
15. Whiteaker P, Sharples CG, Wonnacott S: **Agonist-induced up-regulation of α4β2 nicotinic acetylcholine receptors in M10 cells: pharmacological and spatial definition.** *Mol Pharmacol* 1998, **53**:950-962.
16. Jett DA, Beckles RA, Navoa RV, McLemore GL: **Increased high-affinity nicotinic receptor-binding in rats exposed to lead during development.** *Neurotoxicol Teratol* 2002, **24**:805-811.
17. Karadsheh MS, Shah MS, Tang X, Macdonald RL, Stitzel JA: **Functional characterization of mouse α4β2 nicotinic acetylcholine receptors stably expressed in HEK293T cells.** *J Neurochem* 2004, **91**:1138-1150.
18. Person AM, Bills KL, Liu H, Botting SK, Lindstrom J, Wells GB: **Extracellular domain nicotinic acetylcholine receptors formed by α4 and β2 subunits.** *J Biol Chem* 2005, **280**:39990-40002.
19. Swillens S: **Interpretation of binding curves obtained with high receptor concentrations: practical aid for computer analysis.** *Mol Pharmacol* 1995, **47**:1197-1203.
20. Marks MJ, Meinerz NM, Drago J, Collins AC: **Gene targeting demonstrates that α4 nicotinic acetylcholine receptor subunits contribute to expression of diverse [^{3}H]epibatidine binding sites and components of biphasic $^{86}Rb^+$ efflux with high and low sensitivity to stimulation by acetylcholine.** *Neuropharmacology* 2007, **53**:390-405.
21. Nelson ME, Kuryatov A, Choi CH, Zhou Y, Lindstrom J: **Alternate stoichiometries of α4β2 nicotinic acetylcholine receptors.** *Mol Pharmacol* 2003, **63**:332-341.
22. Marks MJ, Whiteaker P, Calcaterra J, Stitzel JA, Bullock AE, Grady SR, Picciotto MR, Changeux J-P, Collins AC: **Two pharmacologically distinct components of nicotinic receptor-mediated rubidium efflux in mouse brain require the β2 subunit.** *J Pharmacol Exp Ther* 1999, **289**:1090-1103.
23. Butt CM, Hutton SR, Marks MJ, Collins AC: **Bovine serum albumin enhances nicotinic acetylcholine receptor function in mouse thalamic synaptosomes.** *J Neurochem* 2002, **83**:48-56.
24. Buisson B, Bertrand D: **Chronic exposure to nicotine upregulates the human α4β2 nicotinic acetylcholine receptor function.** *J Neurosci* 2001, **21**:1819-1829.
25. Zwart R, Vijverberg HP: **Four pharmacologically distinct subtypes of α4β2 nicotinic acetylcholine receptor expressed in *Xenopus laevis* oocytes.** *Mol Pharmacol* 1998, **54**:1124-1131.
26. Sidach SS, Fedorov NB, Lippiello PM, Bencherif M: **Development and optimization of a high-throughput electrophysiology assay for neuronal α4β2 nicotinic receptors.** *J Neurosci Methods* 2009, **182**:17-24.
27. Vallejo YF, Buisson B, Bertrand D, Green WN: **Chronic nicotine exposure upregulates nicotinic receptors by a novel mechanism.** *J Neurosci* 2005, **25**:5563-5572.
28. Moroni M, Zwart R, Sher E, Cassels BK, Bermudez I: **α4β2 nicotinic receptors with high and low acetylcholine sensitivity: pharmacology, stoichiometry, and sensitivity to long-term exposure to nicotine.** *Mol Pharmacol* 2006, **70**:755-768.
29. Briggs CA, Gubbins EJ, Putman CB, Thimmapaya R, Meyer MD, Surowy CS: **High- and low-sensitivity subforms of α4β2 and α3β2 nAChRs.** *Journal of Molecular Neuroscience* 2006, **30**:11-12.
30. Zhou Y, Nelson ME, Kuryatov A, Choi C, Cooper J, Lindstrom J: **Human α4β2 acetylcholine receptors formed from linked subunits.** *J Neurosci* 2003, **23**:9004-9015.
31. Covernton PJO, Connolly JG: **Multiple components in the agonist concentration-response relationships of neuronal nicotinic acetylcholine receptors.** *J Neurosci Methods* 2000, **96**:63-70.
32. Kuryatov A, Luo J, Cooper J, Lindstrom J: **Nicotine acts as a pharmacological chaperone to up-regulate human α4β2 acetylcholine receptors.** *Mol Pharmacol* 2005, **68**:1839-1851.
33. Zwart R, Broad LM, Xi Q, Lee M, Moroni M, Bermudez I, Sher E: **5-I A-85380 and TC-2559 differentially activate heterologously expressed α4β2 nicotinic receptors.** *Eur J Pharmacol* 2006, **539**:10-17.
34. Tapia L, Kuryatov A, Lindstrom J: **Ca^{2+} permeability of the $(\alpha4)_3(\beta2)_2$ stoichiometry greatly exceeds that of $(\alpha4)_2(\beta2)_3$ human acetylcholine receptors.** *Mol Pharmacol* 2007, **71**:769-776.
35. Anderson DJ, Malysz J, Grønlien JH, El Kouhen R, Håkerud M, Wetterstrand C, Briggs CA, Gopalakrishnan M: **Stimulation of dopamine release by nicotinic acetylcholine receptor ligands in rat brain slices correlates with the profile of high, but not low, sensitivity alpha4beta2 subunit combination.** *Biochem Pharmacol* 2009, **78**:844-851.
36. Carbone AL, Moroni M, Groot-Kormelink PJ, Bermudez I: **Pentameric concatenated $(\alpha4)_2(\beta2)_3$ and $(\alpha4)_3(\beta2)_2$ nicotinic acetylcholine receptors: subunit arrangement determines functional expression.** *Br J Pharmacol* 2009, **156**:970-981.

37. Exley R, Moroni M, Sasdelli F, Houlihan LM, Lukas RJ, Sher E, Zwart R, Bermudez I: **Chaperone protein 14-3-3 and protein kinase A increase the relative abundance of low agonist sensitivity human α4β2 nicotinic acetylcholine receptors in *Xenopus* oocytes.** *J Neurochem* 2006, **98**:876-885.
38. Houlihan LM, Slater Y, Guerra DL, Peng JH, Kuo YP, Lukas RJ, Cassels BK, Bermudez I: **Activity of cytisine and its brominated isosteres on recombinant human α7, α4β2 and α4β4 nicotinic acetylcholine receptors.** *J Neurochem* 2001, **78**:1029-1043.
39. Khiroug SS, Khiroug L, Yakel JL: **Rat nicotinic acetylcholine receptor α2β2 channels: comparison of functional properties with α4β2 channels in *Xenopus* oocytes.** *Neuroscience* 2004, **124**:817-822.
40. Gotti C, Moretti M, Meinerz NM, Clementi F, Gaimarri A, Collins AC, Marks MJ: **Partial deletion of the nicotinic cholinergic receptor α4 or β2 subunit genes changes the acetylcholine sensitivity of receptor-mediated $^{86}Rb^{+}$ efflux in cortex and thalamus and alters relative expression of α4 and β2 subunits.** *Mol Pharmacol* 2008, **73**:1796-1807.
41. Li P, Steinbach JH: **The neuronal nicotinic α4β2 receptor has a high maximal probability of being open.** *Br J Pharmacol* 2010, **160**:1906-1915.
42. Houghtling RA, Dávila-García MI, Kellar KJ: **Characterization of (±)-[^{3}H] epibatidine binding to nicotinic cholinergic receptors in rat and human brain.** *Mol Pharmacol* 1995, **48**:280-287.
43. Marks MJ, Whiteaker P, Collins AC: **Deletion of the α7, β2, or β4 nicotinic receptor subunit genes identifies highly expressed subtypes with relatively low affinity for [^{3}H]epibatidine.** *Mol Pharmacol* 2006, **70**:947-959.
44. Srivastava S, Hamouda AK, Pandhare A, Duddempudi PK, Sanghvi M, Cohen JB, Blanton MP: **[^{3}H]Epibatidine photolabels non-equivalent amino acids in the agonist binding site of Torpedo and α4β2 nicotinic acetylcholine receptors.** *J Biol Chem* 2009, **284**:24939-24947.
45. Hulme EC, Trevethick MA: **Ligand binding assays at equilibrium: validation and interpretation.** *Br J Pharmacol* 2010, **161**:1219-1237.
46. Chanvorachote B, Nimmannit U, Muangsiri W, Kirsch L: **An evaluation of a fluorometric method for determining binding parameters of drug-carrier complexes using mathematical models based on total drug concentration.** *J Fluoresc* 2009, **19**:747-753.
47. Andujar-Sánchez M, Jara-Perez V, Cobos ES, Cámara-Artigas A: **A thermodynamic characterization of the interaction of 8-anilino-1-naphthalenesulfonic acid with native globular proteins: the effect of the ligand dimerization in the analysis of the binding isotherms.** *J Mol Recognit* 2011, **24**:548-556.
48. Beyer WH: *Standard Mathematical Tables* Cleveland, Ohio: CRC Press; 1976.
49. Motulsky HJ, Ransnas LA: **Fitting curves to data using nonlinear regression: a practical and nonmathematical review.** *FASEB J* 1987, **1**:365-374.
50. Cuatrecasas P, Hollenberg MD: **Membrane receptors and hormone action.** *Adv Protein Chem* 1976, **30**:251-451.
51. Cheng Y, Prusoff WH: **Relationship between the inhibition constant (K_i) and the concentration of inhibitor which causes 50 per cent inhibition (I_{50}) of an enzymatic reaction.** *Biochem Pharm* 1973, **22**:3099-3108.
52. Xiao Y, Kellar KJ: **The comparative pharmacology and up-regulation of rat neuronal nicotinic receptor subtype binding sites stably expressed in transfected mammalian cells.** *J Pharmacol Exp Ther* 2004, **310**:98-107.
53. Mendel CM, Mendel DB: **'Non-specific' binding. The problem, and a solution.** *Biochem J* 1985, **228**:269-272.
54. Reed RG: **Spurious cell surface receptors: inadequate correction for saturable, nonspecific binding mimics receptor binding.** *Anal Biochem* 1990, **185**:160-163.
55. McLure JA, Miners JO, Birkett DJ: **Nonspecific binding of drugs to human liver microsomes.** *Br J Clin Pharmacol* 2000, **49**:453-461.
56. Burnham KP, Anderson DR: *Model selection and multimodel inference: A practical information-theoretic approach.* second edition. New York: Springer; 2002.
57. Ludden TM, Beal SL, Sheiner LB: **Comparison of the Akaike information criterion, the Schwarz criterion and the *F* test as guides to model selection.** *J Pharmacokinet Biopharm* 1994, **22**:431-445.
58. Johnson ML, Frasier SG: **Nonlinear least-squares analysis.** *Methods Enzymol* 1985, **117**:301-342.
59. Kishi M, Steinbach JH: **Role of the agonist binding site in up-regulation of neuronal nicotinic α4β2 receptors.** *Mol Pharmacol* 2006, **70**:2037-2044.
60. Sallette J, Pons S, Devillers-Thiery A, Soudant M, Prado de Carvalho L, Changeux J-P, Corringer P-J: **Nicotine upregulates its own receptors through enhanced intracellular maturation.** *Neuron* 2005, **46**:595-607.
61. Gahring LC, Vasquez-Opazo GA, Rogers SW: **Choline promotes nicotinic receptor α4 + β2 up-regulation.** *J Biol Chem* 2010, **285**:19793-19801.

doi:10.1186/2046-1682-4-19
Cite this article as: Person and Wells: Characterizing low affinity epibatidine binding to α4β2 nicotinic acetylcholine receptors with ligand depletion and nonspecific binding. *BMC Biophysics* 2011 **4**:19.